

TYPE-ONE PROTEIN PHOSPHATASE4 Regulates Pavement Cell Interdigitation by Modulating PIN-FORMED1 Polarity and Trafficking in *Arabidopsis*¹

Xiaola Guo², Qianqian Qin², Jia Yan, Yali Niu, Bingyao Huang, Liping Guan, Yuan Li, Dongtao Ren, Jia Li, and Suiwen Hou^{*}

Ministry of Education Key Laboratory of Cell Activities and Stress Adaptations, School of Life Sciences, Lanzhou University, Lanzhou 730000, China (X.G., Q.Q., J.Y., Y.N., B.H., L.G., J.L., S.H.); and State Key Laboratory of Plant Physiology and Biochemistry, College of Biological Sciences, China Agricultural University, Beijing 100193, China (Y.L., D.R.)

In plants, cell morphogenesis is dependent on intercellular auxin accumulation. The polar subcellular localization of the PIN-FORMED (PIN) protein is crucial for this process. Previous studies have shown that the protein kinase PINOID (PID) and protein phosphatase6-type phosphatase holoenzyme regulate the phosphorylation status of PIN1 in root tips and shoot apices. Here, we show that a type-one protein phosphatase, TOPP4, is essential for the formation of interdigitated pavement cell (PC) pattern in *Arabidopsis* (*Arabidopsis thaliana*) leaf. The dominant-negative mutant *topp4-1* showed severely inhibited interdigitated PC growth. Expression of *topp4-1* gene in wild-type plants recapitulated the PC defects in the mutant. Genetic analyses suggested that *TOPP4* and *PIN1* likely function in the same pathway to regulate PC morphogenesis. Furthermore, colocalization, *in vitro* and *in vivo* protein interaction studies, and dephosphorylation assays revealed that TOPP4 mediated PIN1 polar localization and endocytic trafficking in PCs by acting antagonistically with PID to modulate the phosphorylation status of PIN1. In addition, TOPP4 affects the cytoskeleton pattern through the Rho of Plant GTPase-dependent auxin-signaling pathway. Therefore, we conclude that TOPP4-regulated PIN1 polar targeting through direct dephosphorylation is crucial for PC morphogenesis in the *Arabidopsis* leaf.

Polarity is a fundamental characteristic underlying various cellular processes. In plants, cell polarity and morphogenesis are closely linked to the development and function of certain cells in their corresponding tissues and organs. *Arabidopsis* (*Arabidopsis thaliana*) leaf pavement cells (PCs), which have a jigsaw puzzle shape, provide a representative model to study the mechanisms of plant cell polarity and morphogenesis (Yang, 2008; Qian et al., 2009). The interdigitated lobes and indentations of PCs result from intercalary growth (Fu et al., 2005). The cell polarity and morphogenesis are dependent on cell adhesion, signaling networks, the cytoskeleton, and protein transport (Falbel et al., 2003; Mathur et al., 2003; Fu et al., 2005; Wang et al., 2007; Chary et al., 2008; Xu et al., 2010; Li et al., 2013). A well-known mechanism

that controls interdigitated growth of PCs is Rho of Plant (ROP) GTPase-mediated cytoskeletal reorganization in *Arabidopsis* (Fu et al., 2002, 2005, 2009). The cytoskeleton is thought to be critical for the PC shape. Cortical filamentous actins (F-actins) are localized to lobe sites and promote lobe initiation and outgrowth, whereas highly ordered cortical microtubules (MTs) are arranged transversely in the neck regions and restrict cell expansion (Fu et al., 2005). In PC lobes, activated ROP2 and ROP4 act redundantly to promote lobe growth via activation of ROP-interactive Cdc42- and Rac-interactive binding motif-containing protein4 (RIC4)-mediated assembly of cortical diffuse F-actins, and also by suppressing RIC1-mediated organization of cortical MT arrays (Fu et al., 2005). In the indentations of PCs, activated ROP6 interacts with RIC1 to promote well-ordered MTs and suppress lateral expansion (Fu et al., 2009). Recently, it was reported that katanin (KATANIN1) is a downstream component of RIC1, which promotes MT-severing activity by interacting with RIC1 in *Arabidopsis* PCs (Lin et al., 2013).

Auxin is a fundamental plant hormone that regulates many aspects of plant development and mediates various cellular responses (Wu et al., 2011). Treatment of plants with the synthetic auxin naphthalene acetic acid (NAA) promotes PC lobe formation, while quadruple *yucca* mutants with defects in auxin biosynthesis exhibit reduced PC interdigitation (Xu et al., 2010; Li et al., 2011). More recent studies have revealed that both a plasma

¹ This work was supported by the National Basic Research Program of China (grant nos. 2011CB915401 and 2009CB941501), the Natural Science Foundation of China (grant nos. 91017002, 31070247, and 31271460), the Ministry of Agriculture of the People's Republic of China (grant no. 2013ZX08009-003-002), and the Fundamental Research Funds for the Central Universities (grant no. lzujbky-2013-240).

² These authors contributed equally to the article.

* Address correspondence to housw@lzu.edu.cn.

The author responsible for distribution of materials integral to the findings presented in this article in accordance with the policy described in the Instructions for Authors (www.plantphysiol.org) is: Suiwen Hou (housw@lzu.edu.cn).

www.plantphysiol.org/cgi/doi/10.1104/pp.114.249904

membrane-localized transmembrane kinase (TMK) and an auxin binding protein1 (ABP1) form an auxin-sensing complex at cell surface to activate ROP GTPase signaling (Xu et al., 2014). The auxin gradient modulates the ROP-RIC pathway through the ABP1-TMK complex in PCs (Xu et al., 2010, 2014). Auxin is transported from the sites of synthesis to the sites of action via polarized transporters. Polar subcellular localization of the PIN-FORMED (PIN) family proteins directs auxin flow and establishes an auxin gradient (Petrásek et al., 2006; Wisniewska et al., 2006). Reversible protein phosphorylation and dephosphorylation mediated by protein kinases and phosphatases play an essential role in regulating PIN1 polarity and trafficking (Friml et al., 2004; Michniewicz et al., 2007; Kleine-Vehn et al., 2009; Huang et al., 2010). In root and shoot regions, PINOID (PID), a protein Ser/Thr kinase, directly phosphorylates PIN proteins and regulates their polar targeting (Benjamins et al., 2001; Michniewicz et al., 2007). A *pid* loss-of-function mutant causes an apical-to-basal shift in PIN polarity in shoot meristem, whereas the gain-of-function *PID* results in the opposite PIN polarity shift (basal to apical). The type-A regulatory subunit of protein phosphatase2A (PP2A) and PID act antagonistically on PIN phosphorylation and polarity (Michniewicz et al., 2007). Recently, it was found that the corresponding PP6-type heterotrimeric holoenzyme complex, consisting of PP2AA, SAL (for Sit4-associated protein [SAP] subunits domain-like), and FyPP1 (phytochrome-associated Ser/Thr protein phosphatase), directly regulates the phosphorylation status of PIN proteins and consequently affects their polarity (Dai et al., 2012). In addition, PP2A and PID influence brefeldin A (BFA)-independent PIN1 endocytosis in roots (Kleine-Vehn et al., 2009). In *Arabidopsis* PCs, PIN1 is preferentially localized to the plasma membrane of the lobe regions and is essential for PC morphogenesis (Xu et al., 2010; Li et al., 2011). Overexpression of *PIN1* promotes lobe formation, whereas a *pin1* mutant produces PCs devoid of lobes (Xu et al., 2010). Recent report shows that the polar localization of PIN1 modulates PC interdigitation, and PID- and FyPP1-dependent PIN1 phosphorylation affects PIN1 polarity in PCs (Li et al., 2011). However, how the phosphorylated PIN1 in PCs is dephosphorylated remains elusive.

In mammals, PP1 is a major Ser/Thr phosphatase that regulates multiple cellular processes, including cell division, cytoskeletal reorganization, metabolism, synaptic plasticity, transcription, and translation (Shi, 2009). A critical role of PP1 in epithelial cell polarity is regulating the phosphorylation status of a polarity scaffold Partitioning defective3 (Traweger et al., 2008). The catalytic subunit of PP1 is highly conserved, with approximately 70% or greater protein sequence identity among all eukaryotes (Shi, 2009). It is likely that PP1 is also required for plant cell polarity and morphogenesis. In *Arabidopsis*, nine *type-one protein phosphatase* (TOPP) genes encoding the catalytic subunits of PP1 have been cloned (Smith and Walker, 1993; Lin et al., 1998). However, their functions are still poorly understood. In this study, we

characterized a unique function of TOPP4 in regulating PC morphogenesis in *Arabidopsis*. Genetic data suggest that TOPP4 acts antagonistically with PID in regulating PC development. Biochemical analyses demonstrated that TOPP4 directly interacts with and dephosphorylates PIN1, which is crucial for PIN1 polar localization and endocytic trafficking.

RESULTS

The *topp4-1* Mutant Displays Severe PC Defects

In our previous work, we identified a severely dwarfed dominant-negative mutant *topp4-1* and found that TOPP4 acts as a positive regulator in GA signaling through dephosphorylating DELLA proteins (Qin et al., 2014). The *topp4-1* mutant was also found to show PC defects. Analyses of the tissue-specific expression using *TOPP4:TOPP4-GFP* plants showed that TOPP4 is also expressed in leaf PCs (Supplemental Fig. S1). When the mutant was backcrossed to ecotype Columbia, the PC shape of F2 population resulting from self-pollination had a segregation ratio of 94:247:109 (normal PC:moderate PC defect:serious PC defect), which was close to the expected 1:2:1 segregation ratio for a semidominant single locus. The rosette leaves of *topp4-1* mutant were small, narrow, and curly (Supplemental Fig. S2, A and D). PCs, stomata, and trichomes were all present in the *topp4-1* mutant, suggesting that the mutation did not affect cell differentiation in leaves. PCs on abaxial and adaxial leaf surfaces in the wild type are shaped like a jigsaw puzzle with lobes and necks that interlock with those of adjacent cells (Fig. 1A). In the *topp4-1* mutant, the PC shape in cotyledons and the first and second true leaves was similar to those in the wild-type plants (Supplemental Fig. S3). However, after the third leaves, the PCs had either no lobes or less pronounced lobes in the mutant (Fig. 1A). The outlines of PCs in *topp4-1* were straighter than those in the wild-type plants and similar to those in *rop4-1 ROP2 RNA interference* (*R2i-34*) or *RIC1-OVEREXPRESSION* (*OX*) mutants (Fu et al., 2005). The lobe number and length as well as the neck width of PCs in *topp4-1* were reduced dramatically (Fig. 1, B–D). The average PC area was also dramatically reduced in *topp4-1* compared with that of the wild type (Supplemental Fig. S2E). Circularity has been used as a key parameter to characterize PC geometry, which is independent of its size (Dewitte et al., 2003). Using the geometric analytical method (Guo et al., 2013), we found larger values of circularity in *topp4-1* PCs (Fig. 1E), indicating that the reduced lobe length of PCs in *topp4-1* was not the result of a decrease in cell size. Transverse sections of mature rosette leaves indicated that more cells were produced in *topp4-1*, the palisade cell size was smaller, and the shapes of palisade and sponge mesophyll cells were indistinguishable (Supplemental Fig. S2, B and C).

Next, we performed a time course analysis of PC development in the *topp4-1* mutant. The development of *Arabidopsis* leaf PCs is separated into three stages (Fu et al., 2002). In the first phase, wild-type PCs were mostly

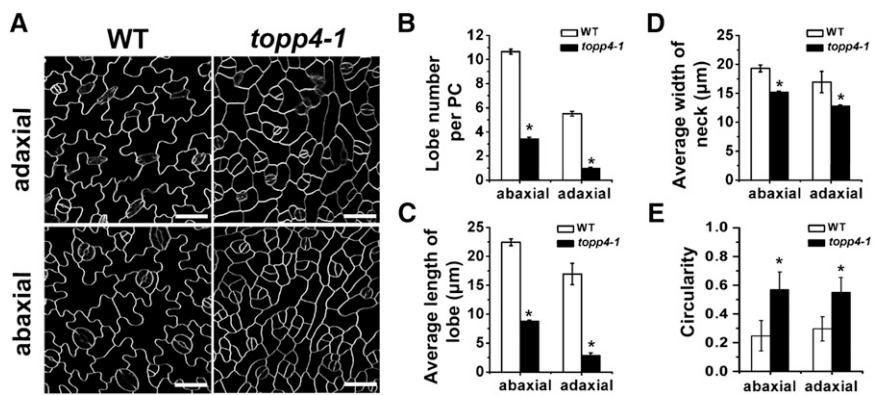


Figure 1. The *topp4-1* mutant shows aberrant PC shape. A, PCs on the abaxial and adaxial leaf sides in the wild type (WT) and *topp4-1*. Bars = 50 μ m. B, The average lobe number per PC in *topp4-1* was fewer than the wild type. C, The average lobe length of *topp4-1* PCs was significantly reduced compared with that of the wild type. D, The average neck width of *topp4-1* PCs was significantly reduced compared with that of the wild type. E, The circularity values of PCs in the wild type and *topp4-1*. Asterisks in B to E represent statistical differences from the wild type based on Student's *t* test with $P < 0.01$. Error bars represent se ($n = 100$).

square, rectangular, or pentagonal, but some cells were slightly more expanded (Supplemental Fig. S4A). PCs of the *topp4-1* mutant were similar to those of the wild-type plants at this stage (Supplemental Fig. S4D). At stage II, wild-type PCs had apparent lobes and one or more necks along the long axis, whereas *topp4-1* PCs continued to expand and had no visible lobes (Supplemental Fig. S4, B and E). Subsequently, stage II wild-type PCs expanded largely in the direction of the PC long axis, resulting in highly lobed interlocking stage III cells (Supplemental Fig. S4C). However, at stage III, lobes appeared to form in *topp4-1* PCs, but they were much less obvious than that in wild-type PCs (Supplemental Fig. S4F). These results showed that *TOPP4* might be involved in the lobe formation and outgrowth of PCs.

Overexpression of *TOPP4* in the *topp4-1* Mutant Rescues the PC Defects, and Its Overexpression in Wild-Type Plants Promotes PC Interdigitated Growth

To confirm whether the single nucleotide substitution in *TOPP4* is responsible for the defective PC phenotype, we observed four independent 35S:*TOPP4* *topp4-1* T1-transformed lines (Qin et al., 2014). Three lines (*complement* [COM] 1#–COM 3#) showed a completely recovered PC phenotype (Fig. 2, A–E). One line (COM 4#) had a weak complemented phenotype (Fig. 2F). Quantitative PCR analysis indicated that COM 4# had a lower overexpression level of *TOPP4* than the other three lines (Fig. 2I). Therefore, it appeared that the recovery effect on PCs was positively correlated with the expression level of *TOPP4* gene in *topp4-1*. We also analyzed PC morphology of five individual *TOPP4*:*TOPP4* *topp4-1*-transformed lines (Qin et al., 2014). They all showed a slightly recovered PC phenotype (two lines are showed in Supplemental Fig. S5) with a deeper and larger number of lobes than the *topp4-1* mutant, but the PCs in the transformed lines still displayed

shallower lobes than the wild type (Supplemental Fig. S5). Taken together, these results demonstrated that *TOPP4* is responsible for the leaf PC defect in the *topp4-1* mutant.

In addition, two transfer DNA insertion lines of *TOPP4*, SALK_090980, and N466328 did not show any obvious PC defects (Qin et al., 2014; Supplemental Fig. S6), possibly due to the high expression level of *TOPP4* in these two lines or functional redundancy among *TOPP* genes.

To further investigate the function of *TOPP4* in PC morphology, two representative *TOPP4*-overexpressing transgenic lines with the highest expression level of *TOPP4* (lines 4# and 6#) were selected for further phenotypic analyses (Qin et al., 2014; Supplemental Fig. S7A). These two lines exhibited longer and more frequent lobes as well as a wider neck than the wild-type plants (Fig. 2, G, H, J, and K), confirming that *TOPP4* promotes lobe outgrowth and lateral expansion of PCs. The representative transgenic lines with the highest expression level of *TOPP4* (6#) were selected for further analysis and renamed as 35S:*TOPP4*.

Expression of *topp4-1* in Wild-Type Plants Recapitulates the PC Defects of the *topp4-1* Mutant, and Inhibition of PP1 Hinders Interdigitated Growth of PCs

To verify whether the mutant *topp4-1* protein had a dominant-negative effect on PC growth, we first analyzed three *TOPP4*:*topp4-1*-GFP lines (Qin et al., 2014). Constitutive expression of *topp4-1* in these lines was confirmed by quantitative reverse transcription (qRT)-PCR (Supplemental Fig. S7B). The representative transgenic line (1#) with the highest expression level was selected for further phenotypic analyses, which recapitulated the PC defects of *topp4-1*, as characterized by a reduced lobe length and neck width (Fig. 3). We also observed the phenotypes of the 35S:*topp4-1*-GFP

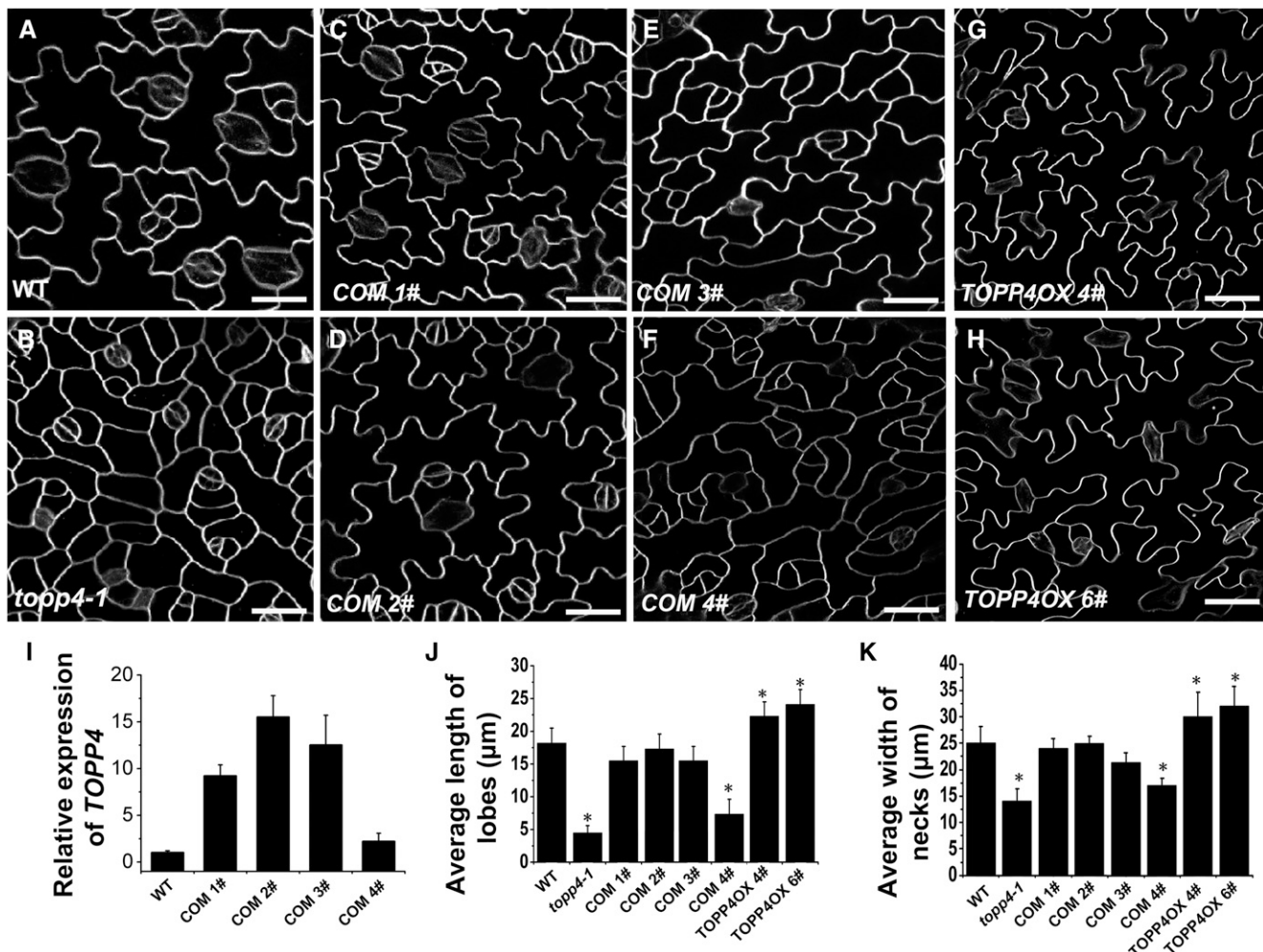


Figure 2. Overexpression of *TOPP4* in *topp4-1* complements the mutant PC defect, while its overexpression promotes interdigitated PC growth. A to H, PCs on the adaxial leaf side in the wild type (WT), *topp4-1*, four complemented lines (COM 1#–COM 4#), and two *TOPP4* overexpression lines (TOPP4OX 4# and TOPP4OX 6#). Bars = 25 μ m. I, The relative expression levels of *TOPP4* in four complemented lines shown in C to F. The expression level of *TOPP4* in the wild type was set to 1.0. J and K, Quantitative analyses of lobe length (J) and neck width (K) in the wild type, *topp4-1*, four complemented lines (COM 1#–COM 4#), and two *TOPP4* overexpression lines (TOPP4OX 4# and TOPP4OX 6#). Asterisks indicate significant difference from the wild type ($P < 0.01$ by Student's *t* test). Error bars represent SE ($n = 100$).

transgenic lines (Qin et al., 2014). The PCs of all overexpression lines were highly reminiscent of the *topp4-1* mutant (line 3# with the highest expression level was displayed in Supplemental Fig. S7C and Fig. 3). These results suggest that *topp4-1* affects PC development in a dominant-negative fashion.

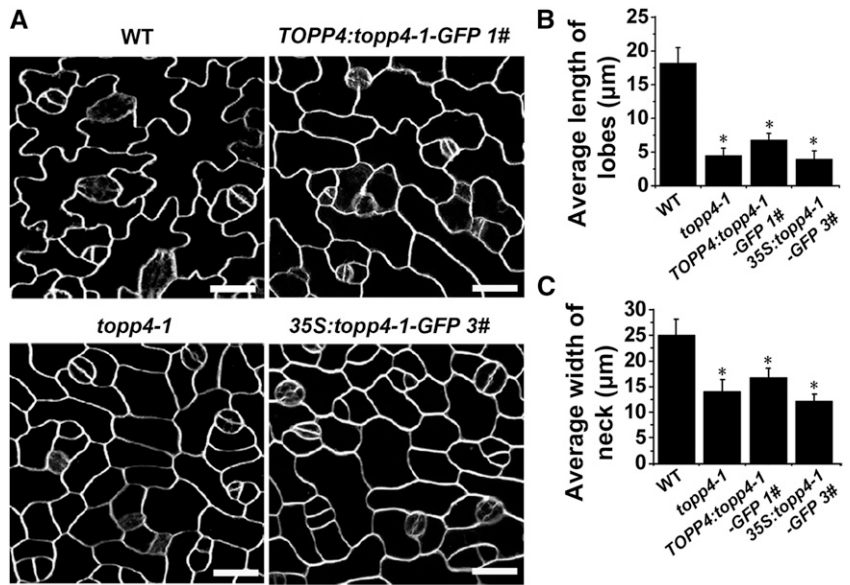
It has been reported that tautomycin is a specific inhibitor of PP1, because it inhibits PP2A with 10-fold lower sensitivity in vitro (Favre et al., 1997; Takemiyia et al., 2006). Similar to mammalian PP1 phosphatases, Arabidopsis TOPP phosphatases are potently inhibited by tautomycin (Stubbs et al., 2001). We therefore investigated the effects of tautomycin on the PC morphology of wild-type plants. Treatment with 0.1 μ M tautomycin inhibited the lobe growth and formation of PCs in true leaves (Supplemental Fig. S8), and a higher concentration

of tautomycin (1.0 μ M) strongly inhibited PC growth (Supplemental Fig. S8). These results suggest that TOPP phosphatases are involved in the interdigitated PC growth.

The *topp4-1* Mutant Displays Auxin-Related Phenotypes, and Exogenously Applied Auxin Dose Not Rescue PC Lobe Formation

The phenotypes of the *topp4-1* mutant (i.e. the PC interdigitation defect, reduced apical dominance, increased number of branches, and reduced root length) resemble those in mutants of auxin synthesis, transport, and response (Supplemental Fig. S9, A–C). These defects may be related to the action of auxin. Therefore, we first

Figure 3. Overexpression of *topp4-1* gene in wild-type (WT) plants recapitulates PC phenotype of *topp4-1*. A, PCs on the adaxial leaf side in wild-type, *topp4-1*, *TOPP4:topp4-1-GFP 1#*, and *35S:topp4-1-GFP 3#* plants. Bars = 25 μ m. B and C, Quantitative analyses of lobe length (B) and neck width (C) of PCs in wild-type, *topp4-1*, *TOPP4:topp4-1-GFP 1#*, and *35S:topp4-1-GFP 3#* plants. Asterisks represent statistical differences from the wild type based on Student's *t* test with $P < 0.01$. Error bars represent SE ($n = 100$).

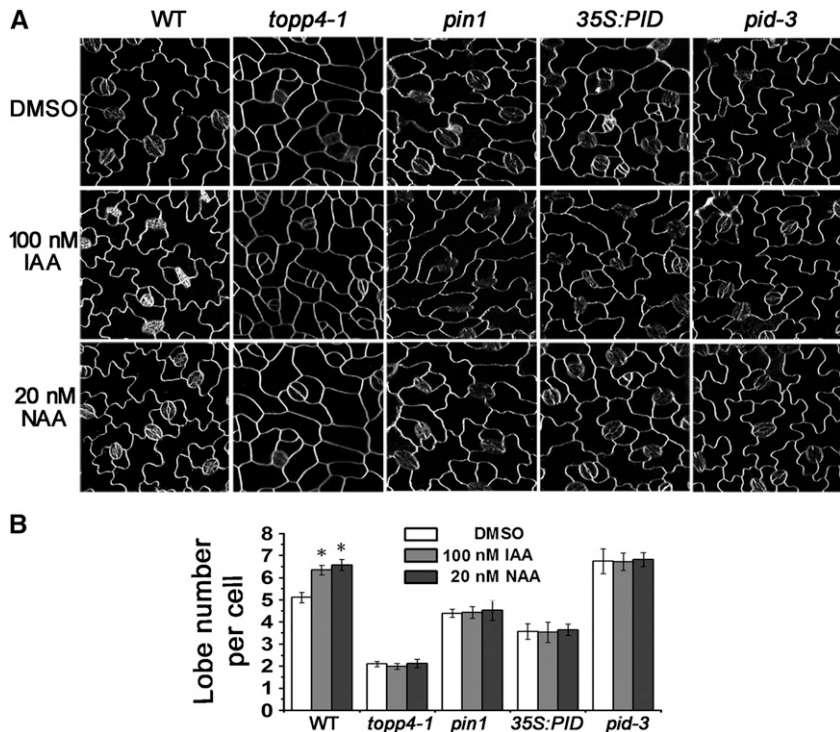


analyzed local auxin distribution in *topp4-1* using the reporter of auxin-responsive promoter DR5 (Ulmasov et al., 1997). In wild-type seedlings, the GUS signal was restricted to the tips of the leaves (Supplemental Fig. S9D). However, GUS-stained areas in *topp4-1* were greatly increased in the leaf tips, and these areas extended up to the leaf margins (Supplemental Fig. S9D). By contrast, the activity of the DR5 reporter was less at the primary root tip of *topp4-1*, but it was significantly higher in *35S:TOPP4* roots than in the wild-type plant roots (Supplemental Fig.

S9E). This result indicated that DR5 activity is affected in the *topp4-1* mutant.

Next, we examined the effect of exogenous auxin on the degree of PC interdigitation. In wild-type plants, the lobe number of PCs was significantly increased by application of exogenous auxin (Fig. 4). The mean number of lobes was increased from 5.14 to approximately 6.5 lobes per cell after 100 nm indole-3-acetic acid (IAA) or 20 nm NAA treatment. However, neither IAA nor NAA treatment rescued PC lobe formation in the *topp4-1* mutant (Fig. 4);

Figure 4. The PC interdigitation in *topp4-1* is not rescued by exogenous auxin. A, PCs on the adaxial leaf side in wild-type (WT), *topp4-1*, *pin1*, *35S:PID*, and *pid-3* plants treated with DMSO, 100 nm IAA, or 20 nm NAA. Bars = 50 μ m. B, Analyses of lobe number per PC in wild-type, *topp4-1*, *pin1*, *35S:PID*, and *pid-3* plants treated with DMSO, 100 nm IAA, or 20 nm NAA. Asterisk represents statistical difference from the untreated wild type based on Student's *t* test with $P < 0.01$. Error bars represent SE ($n = 300$).



similar results were obtained in *pin1*, 35S:*PID*, and *pid-3* mutants (Fig. 4; Xu et al., 2010). Thus, we hypothesized that *TOPP4* is involved in the auxin-promoted PC interdigitation.

TOPP4 Genetically Interacts with *PIN1* and *PID* in PC Interdigitation and Plant Development

A *pin1* mutant, which is defective for auxin transport, has abnormal PC interdigitation in cotyledons and true leaves (Xu et al., 2010). Considering that the PC shape in *topp4-1* mutant is similar to that in the *pin1* mutant, we analyzed the phenotype of *topp4-1 pin1* double mutants to determine whether both *TOPP4* and *PIN1* function genetically in the same pathway. All double mutants generated from self-pollination of *topp4-1 pin1* plants exhibited *pin1* phenotypes (Supplemental Fig. S10). Among the progeny of *pin1*, 12.4% ($n = 646$) of seedlings was defective for the formation of cotyledons and true leaves. However, the overall frequency of aberrant leaf phenotypes was higher in *topp4-1 pin1* progeny, with up to 17.5% ($n = 426$) of seedlings. These results indicate that *topp4-1* enhances *pin1* loss-of-function phenotypes, suggesting that *TOPP4* is involved in *PIN1*-mediated auxin transport. Moreover, most of the adaxial leaf PCs of *topp4-1 pin1* double mutants resembled those of the *pin1* mutant (Fig. 5). Consistently, the PC shape of the

pin1 mutant treated with tautomycin resembled that of the *pin1* mutant (Supplemental Fig. S11). These data indicate that both *TOPP4* and *PIN1* likely function genetically in the same pathway to regulate PC interdigitation and that *PIN1* is located downstream of *TOPP4*.

Compared with the PCs of the wild type, those of the *PID* gain-of-function mutant (35S:*PID*) were significantly decreased in lobe number and length, whereas PCs of the *PID* loss-of-function mutant (*pid-3*) exhibited more frequent and deeper lobes (Fig. 5). The PC defects of the *topp4-1* mutant are similar to those of 35S:*PID*, but opposite to those of the *pid-3* mutant (Fig. 5), suggesting that *TOPP4* and *PID* may have a genetic interaction. To test this hypothesis, we constructed *topp4-1 35S:PID* and *topp4-1 pid-3* double mutants. The *topp4-1 35S:PID* double mutants showed more severe defects in plant development than each single mutant (Supplemental Fig. S12). Some *topp4-1 35S:PID* plants failed to form true leaves and showed arrested growth as seedlings. By contrast, the PC defects of *pid-3* were partially suppressed by *topp4-1* (Fig. 5). The *topp4-1 pid-3* PCs had fewer and shorter lobes than those of *pid-3*. The length of inflorescence stems in the *topp4-1 pid-3* double mutant decreased compared with the *pid-3* single mutant (Supplemental Fig. S13). Additionally, the PC interdigitated growth of 35S:*PID* and *pid-3* mutants was partially inhibited by tautomycin treatment, which is similar to what was observed in *topp4-1 35S:PID* and *topp4-1 pid-3* double

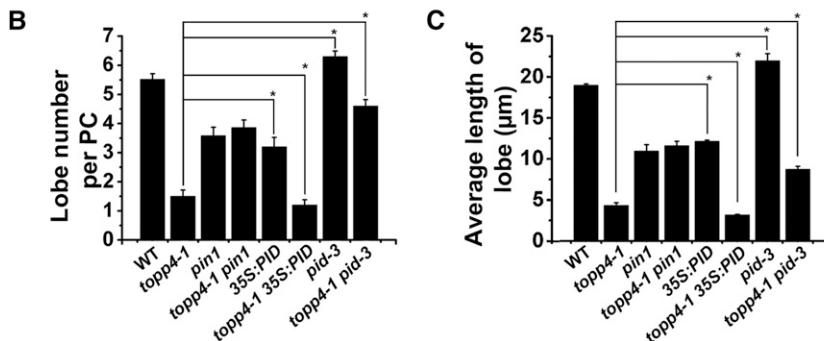
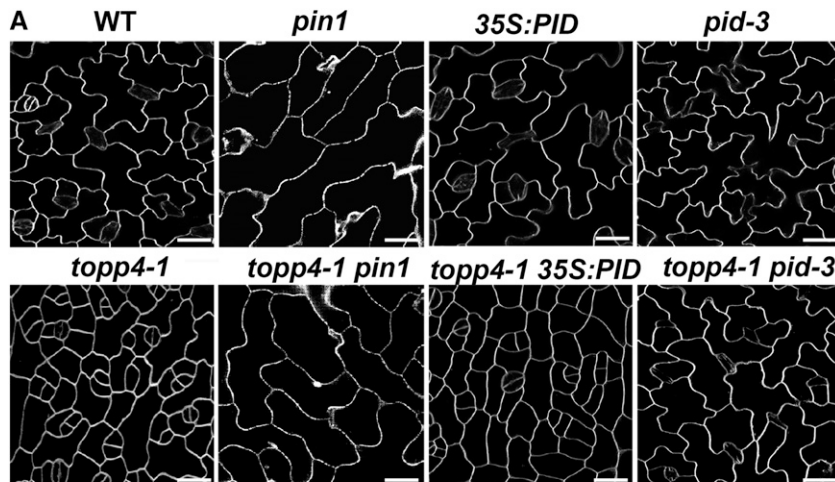


Figure 5. *TOPP4* acts antagonistically with *PID* to regulate leaf PC morphogenesis. A, PCs on the adaxial leaf side in the wild type (WT), *topp4-1*, *pin1*, *topp4-1 pin1*, 35S:*PID*, *topp4-1 35S:PID*, *pid-3*, and *topp4-1 pid-3* double mutants. Bars = 25 μ m. B and C, Quantitative analyses of lobe number (B) and lobe length (C) of PCs. Asterisks represent statistical difference from *topp4-1* based on Student's *t* test with $P < 0.05$. Error bars represent SE ($n = 100$).

mutants (Supplemental Fig. S11). These genetic analyses suggest that *TOPP4* may act antagonistically with *PID* to regulate PC morphogenesis.

TOPP4 Directly Interacts with PIN1 in Vitro and in Vivo

To reveal the subcellular localization of TOPP4 protein, *35S:TOPP4-GFP* was expressed in wild-type Arabidopsis. We found that TOPP4 protein was mainly localized to the nucleus and plasma membrane, and some TOPP4 proteins were found in the cytoplasm (Fig. 6A; Qin et al., 2014). Analyses of TOPP4-GFP expression under

the control of its native promoter in the wild-type plants confirmed the subcellular distribution of TOPP4 protein (Supplemental Fig. S1).

At the subcellular level, PIN1 protein is localized to the plasma membrane (Gälweiler et al., 1998; Michniewicz et al., 2007). Our results showed colocalization of a fraction of TOPP4 with FM4-64 and PIN1 at the plasma membrane (Fig. 6, A and B). Next, we determined whether TOPP4 interacts with PIN1 directly. We examined the interactions of TOPP4 and PIN1 by a series of biochemical approaches. Using a yeast (*Saccharomyces cerevisiae*) two-hybrid assay, TOPP4 was expressed as a DNA-binding domain (BD) fusion protein, and PIN1 was expressed as

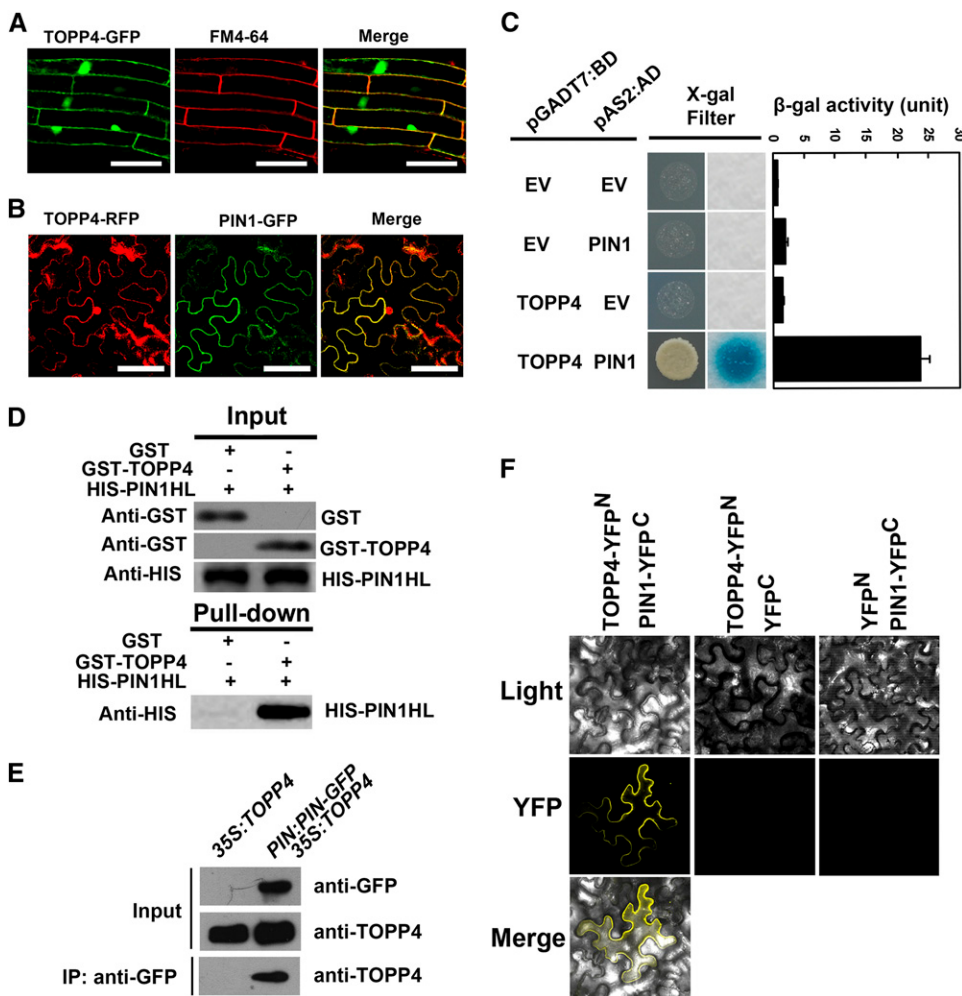


Figure 6. TOPP4 physically interacts with PIN1 protein in vitro and in vivo. A, Subcellular localization of TOPP4-GFP and colocalization of TOPP4-GFP and FM4-64 in Arabidopsis roots. Bars = 100 μ m. B, Colocalization of TOPP4-YFP and PIN1-GFP at the plasma membrane of *N. benthamiana* leaf epidermal cells. Bars = 100 μ m. C, Yeast two-hybrid assay was used to determine the interactions between TOPP4 and PIN1. Quantitative measurements of β -gal activities are shown on the right. Error bars represent se ($n = 3$). X-Gal, 5-Bromo-4-chloro-3-indolyl- β -D-galactopyranoside acid. D, Pull-down assay between GST-TOPP4 and HIS-PIN1. Precipitated HIS-PIN1 was detected by anti-HIS antibody. E, Co-IP of TOPP4 with PIN1-GFP. Membrane extracts of *PIN1:PIN1-GFP 35S:TOPP4* plants were immunoprecipitated with an anti-GFP antibody and detected by immunoblotting using an anti-TOPP4. Immunoprecipitation (IP) by the anti-GFP in *35S:TOPP4* was used as a negative control. F, BiFC assays showed that TOPP4 interacts with PIN1 at plasma membrane. TOPP4-YFP^N and PIN1-YFP^C fusion proteins were expressed in *N. benthamiana* epidermal cells. No YFP signal was detected in negative controls in which either TOPP4-YFP^N or PIN1-YFP^C was coexpressed with the corresponding empty vector (EV). Light indicates bright field, YFP indicates YFP fluorescence, and merge indicates merged view of the light and YFP images.

a transactivation domain (AD) fusion protein in the yeast strain Y190. Interactions of TOPP4-BD and PIN1-AD were confirmed by β -galactosidase (β -gal) activity (Fig. 6C). Recombinant His (HIS)-PIN1 hydrophilic loop (PIN1HL) and glutathione S-transferase (GST)-TOPP4 were purified from *Escherichia coli* and followed by pull-down experiments. HIS-PIN1HL was pulled down together with GST-TOPP4 using glutathione Sepharose 4B resin (Fig. 6D).

Furthermore, to test the interaction of TOPP4 and PIN1 in vivo, we performed coimmunoprecipitation (co-IP) and bimolecular fluorescence complementation (BiFC) assays. We crossed *PIN1:PIN1-GFP* with *35S:TOPP4* to generate *PIN1:PIN1-GFP 35S:TOPP4* for use in co-IP assays. *35S:TOPP4* was used as a negative control. PIN1 protein was immunoprecipitated with an anti-GFP antibody, and PIN1-bound proteins were subjected to immunoblot analysis. As a result, TOPP4 was coimmunoprecipitated with PIN1 in *PIN1:PIN1-GFP 35S:TOPP4*, but not in *35S:TOPP4* (Fig. 6E). When TOPP4-N-terminal yellow fluorescent protein and PIN1-C-terminal yellow fluorescent protein were transiently coexpressed in the leaves of *Nicotiana benthamiana*, strong yellow fluorescent signal was clearly detected at the plasma membrane of PCs (Fig. 6F). Taken together, the above experiments demonstrated that TOPP4 directly interacts with PIN1 in vitro and in vivo.

TOPP4 Directly Dephosphorylates PIN1

Next, we determined whether TOPP4 dephosphorylated PIN1 directly. A previous study has shown that higher M_r bands of endogenous PIN1 appear when *PID* is overexpressed (Michniewicz et al., 2007). Therefore, we isolated wild-type protoplasts and transfected them with *35S:PIN1-GFP* and/or *35S:PID-FLAG*. PIN1-GFP was observed predominantly at the protoplast plasma membrane by a confocal microscopy (Supplemental Fig. S14A). PID-FLAG was detected on protein blots with the expected M_r (Supplemental Fig. S14B). We observed additional signals of PIN1-GFP with a high M_r in protein extracts of protoplasts cotransfected with *35S:PIN1-GFP* and *35S:PID-FLAG* (Fig. 7A). To test whether the observed electrophoretic mobility shift corresponded to PIN1 phosphorylation, we incubated protein extracts from protoplasts that were transiently transfected with the two constructs with λ -phosphatase. The appearance of additional PIN1 bands was sensitive to λ -phosphatase treatment (Fig. 7A), indicating that these additional PIN1-GFP signals with reduced mobility were due to phosphorylation. We also incubated the protein extracts of TOPP4 or mutant *topp4-1*, which were immunoprecipitated from wild-type or *topp4-1* plants, respectively, with anti-TOPP4 antibody. Consistent with the results obtained by λ -phosphatase treatment, the additional PIN1 bands disappeared when treated with TOPP4, but not mutant *topp4-1* (Fig. 7A), indicating that TOPP4 can dephosphorylate PIN1.

Furthermore, we used an in vitro phosphorylation assay to examine the ability of total protein extracts derived

from plant materials to phosphorylate HIS-PIN1HL (Michniewicz et al., 2007; Dhonekshet al., 2010; Dai et al., 2012). We used the hydrophilic loop of PIN1 as the substrate. Equal amounts of recombinant HIS-PIN1HL residues expressed in *E. coli* were coincubated with equal amounts of extracts prepared from wild-type, *35S:PID*, *topp4-1*, or *35S:TOPP4* plants. Consistent with the results of previous reports (Michniewicz et al., 2007; Dai et al., 2012), autoradiograph results in this study showed that the amounts of phosphorylated HIS-PIN1HL residues were significantly higher upon incubation with *35S:PID* protein extracts than that observed after incubation with the wild-type protein extracts (Fig. 7B). Similarly, the amounts of phosphorylated HIS-PIN1HL were evidently higher in protein extracts derived from *topp4-1* plant, but lower in *35S:TOPP4* protein extracts, than in the protein extracts from the wild-type plants (Fig. 7B). These results suggest that the *topp4-1* mutation might reduce PIN1 dephosphorylation.

To test whether PIN1 can be dephosphorylated by TOPP4 in planta, we first compared a migration of PIN1-GFP from wild-type, *topp4-1*, and *35S:TOPP4* plants expressing PIN1-GFP by SDS-PAGE. Immunoblot analysis using an anti-GFP antibody produced a single band of the expected size for PIN1-GFP in all plants (Supplemental Fig. S15). A previous report has shown that higher M_r bands of PIN1 appear on SDS-PAGE (Abas and Luschnig, 2010). Therefore, PIN1-GFP proteins were immunoprecipitated with the anti-GFP antibody from wild-type, *topp4-1*, and *35S:TOPP4* plants expressing PIN1-GFP and then run on SDS-PAGE for immunoblot analysis. A higher accumulation of the slowly migrating forms of PIN1-GFP was observed in *topp4-1* but not in *35S:TOPP4* (Fig. 7C). Moreover, the retarded bands in *topp4-1* were sensitive to λ -phosphatase treatment but stable in the presence of denatured λ -phosphatase (Fig. 7C). These data support the notion that TOPP4 is required for PIN1 dephosphorylation.

To further confirm that TOPP4 dephosphorylates PIN1 directly, we first obtained the phosphorylated HIS-PIN1HL residues by incubating HIS-PIN1HL with GST-PID in an in vitro phosphorylation reaction. Equal amounts of phosphorylated PIN1HL residues were then treated with TOPP4, mutant *topp4-1*, or denatured TOPP4, which were immunopurified from plants. Autoradiographic results showed that phosphorylated HIS-PIN1HL was dephosphorylated by TOPP4, but not by mutant *topp4-1*, or denatured TOPP4 (Fig. 7D). These data support the conclusion that TOPP4 acts antagonistically with PID to dephosphorylate PIN1 protein directly.

TOPP4 Is Required for PIN1 Polarity Maintenance

In PCs, PIN1 protein is preferentially localized to the plasma membrane of the lobe regions, and the PIN1 polarity switch between lobes and indentations is controlled by protein phosphorylation (Xu et al., 2010; Li et al., 2011). PIN1 polarity shifts from lobes to indentations in *35S:PID* and *FYPP1* (a catalytic subunit

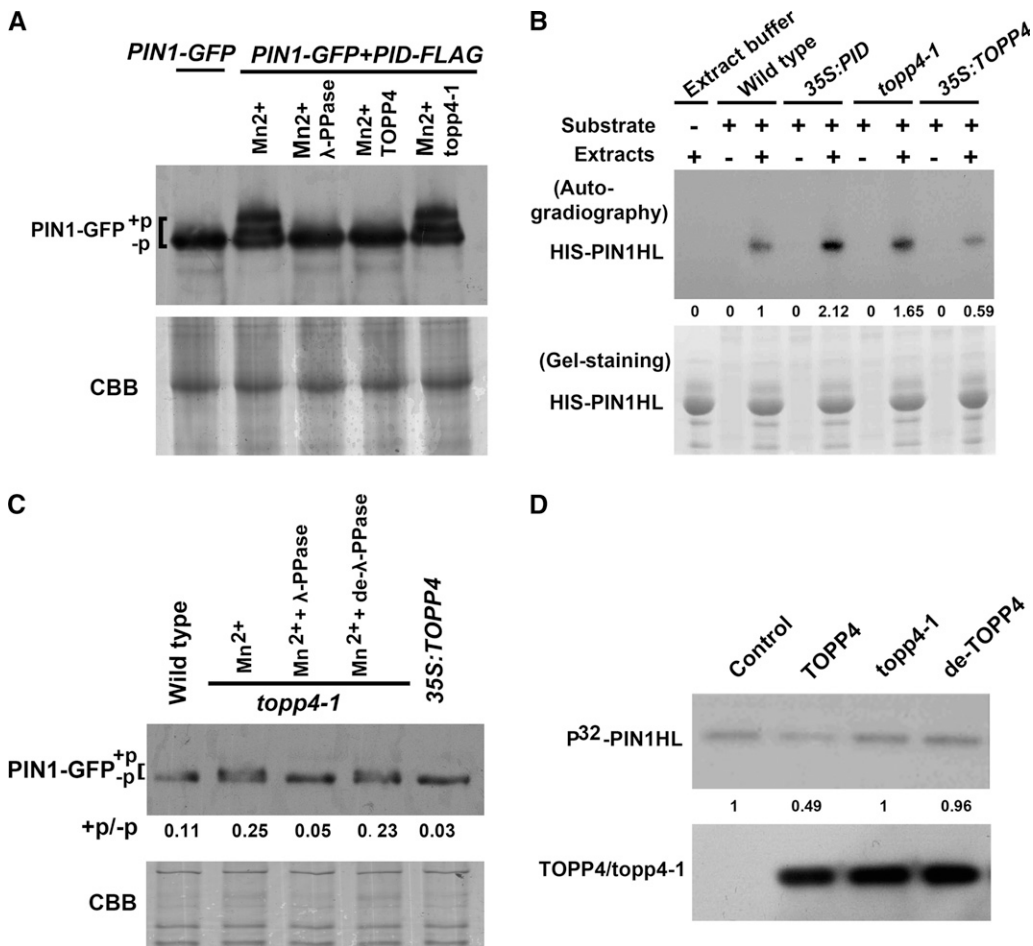


Figure 7. TOPP4 directly dephosphorylates PIN1. **A**, Immunoblot assay of PIN1-GFP protein incubated with λ protein phosphatase (λ -PPase), TOPP4, or mutant *topp4-1*. Western blot demonstrating PIN1-GFP expression in protoplasts transfected with 35S:PIN1-GFP and/or 35S:PID-FLAG. A high M_r of PIN1-GFP signals appeared in cotransfected protoplasts. The appearance of additional PIN1-GFP bands was sensitive to λ -PPase and TOPP4 treatments but stable in the presence of *topp4-1*. **B**, Increased phosphorylation of the HIS-PIN1 by total protein extracts of 35S:PID and *topp4-1* compared with those of the wild type and 35S:TOPP4. Numbers under lanes indicate relative band intensities that were quantified and normalized for each section. **C**, Increased accumulation of higher M_r of PIN1-GFP in *topp4-1* compared with the wild type on SDS-PAGE, whereas the retarded bands did not appear in 35S:TOPP4. These bands were sensitive to λ -PPase treatment but stable in the presence of denatured λ -PPase (de- λ -PPase). **D**, In the top row, HIS-PIN1HL residues were phosphorylated by GST-PID using [γ -³²P] ATP and then incubated with TOPP4, mutant *topp4-1*, or denatured TOPP4. Numbers under lanes indicate relative band intensities that were quantified and normalized for each section. In the bottom row, western blot of the precipitated TOPP4/*topp4-1* proteins using anti-TOPP4 antibody. +P indicates phosphorylated status, and -P indicates dephosphorylated status. +P/-P indicates blot value ratios of phosphorylated PIN1 to unphosphorylated one quantified by ImageJ. CBB, Coomassie Brilliant Blue.

gene of PP6) loss-of-function mutants (Li et al., 2011). To test the effect of TOPP4-mediated PIN1 dephosphorylation on PIN1 localization, we performed an immunolocalization assay in wild-type, *topp4-1*, and 35S:TOPP4 PCs. In wild-type PCs, approximately 70% of the cells had preferential PIN1 localization to the plasma membrane of lobe regions (Fig. 8, A and J), consistent with previous observations (Li et al., 2011). However, in *topp4-1* PCs, the polar localization of PIN1 was much less pronounced, and a significant proportion of PIN1 shifted from the lobes to indentations or nonlobing regions (Fig. 8, B and J). The polar localization of PIN1 was almost unaltered in 35S:TOPP4 PCs, but the number of PCs

with preferential localization of PIN1 to lobe regions in 35S:TOPP4 was higher than that of the wild-type PCs (Fig. 8, C and J).

To investigate whether the polar localization of PIN was also affected in the roots of *topp4-1* and 35S:TOPP4 plants, we crossed them with *PIN1:PIN1-GFP* and *PIN2:PIN2-GFP* marker lines. In wild-type roots, PIN1 was localized preferentially to the basal side of stele cells, while PIN2 was localized at the apical side of epidermis cells and the basal side of cortex cells (Fig. 8, D and G; Blilou et al., 2005). In *topp4-1* stele cells, the basal polarity of PIN1 was much less pronounced, and the number of cells with nonpolar and apical PIN1 was increased

significantly (Fig. 8, E and K). In addition, the basal PIN2 polarity in the cortex cells of *topp4-1* was much less pronounced, but the apical PIN2 localization in epidermis cells was not visibly affected (Fig. 8, H and K). Compared with PID and PP2A mutations, the polar PIN1 and PIN2 shifts in *topp4-1* appeared to be more gradual. In 35S:TOPP4, there was an increase in the proportion of cells with normal PIN1 or PIN2 localization, while the proportion of cells with nonpolar PIN1 or PIN2 decreased (Fig. 8, F, I, and K). Taken together, these observations indicate that TOPP4-mediated PIN dephosphorylation is required for PIN polarity in leaf PCs and root cells.

TOPP4 Is Required for Endocytic Trafficking of PIN1 in PCs

The fungal toxin BFA is useful to investigate early endocytic trafficking (Geldner et al., 2001; Kleine-Vehn

et al., 2008). Recent studies have shown that PIN1-GFP is preferentially internalized in the indentation regions of PCs, and BFA treatment induces large aggregations of PIN1-GFP into BFA bodies (Nagawa et al., 2012). In wild-type root cells, BFA induced PIN1 internalization and formed large aggregates (Kleine-Vehn et al., 2008; Supplemental Fig. S16). However, the effect of BFA on PIN1 localization was severely impaired in *topp4-1*, as manifested by the significantly reduced BFA-induced PIN1 internalization and PIN1 retention at the plasma membrane (Supplemental Fig. S16). In 35S:TOPP4 root cells, BFA rapidly induced PIN1 internalization and formed larger BFA compartments compared with the wild type (Supplemental Fig. S16). To test the effect of TOPP4-dependent PIN1 dephosphorylation on the endocytic trafficking in PCs, we first monitored BFA-induced intracellular accumulation of PIN1 of *topp4-1* and

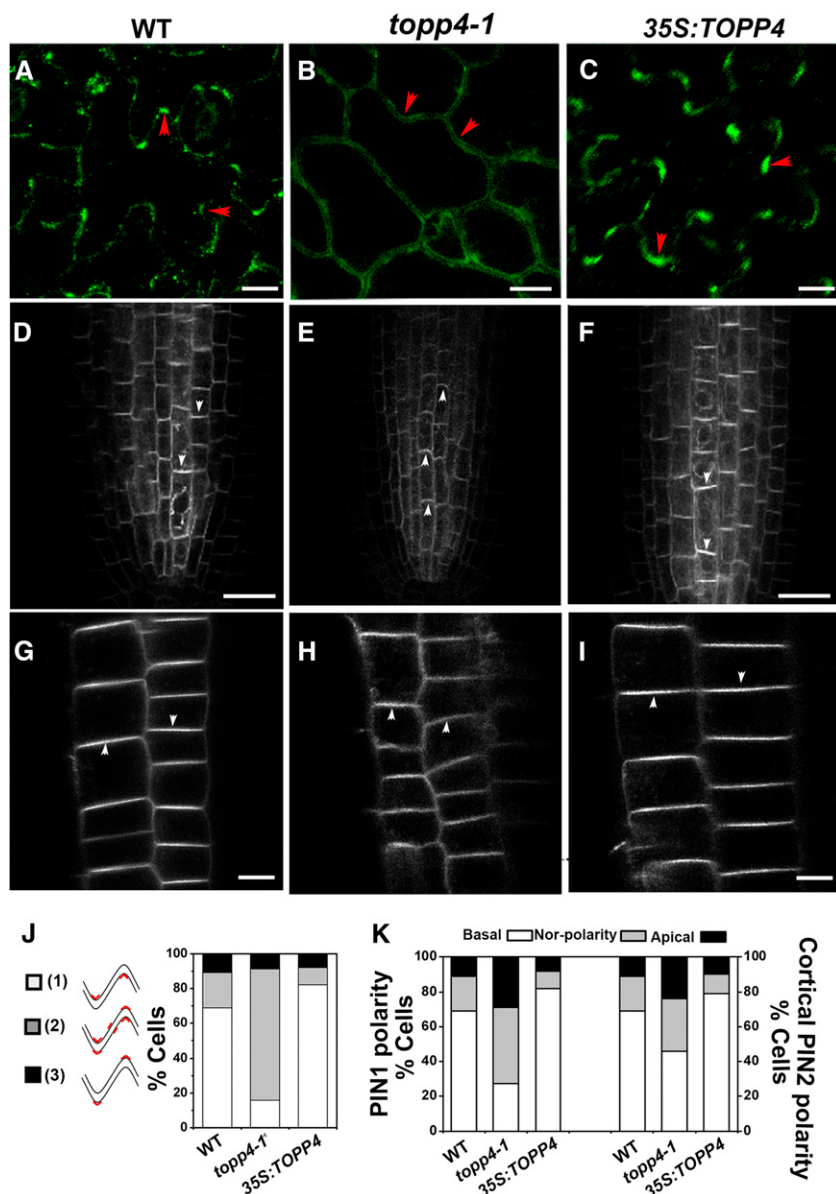


Figure 8. Polar localization of PIN1 and PIN2. A to C, Subcellular localization of PIN1 in PCs was detected by immunofluorescence with the anti-PIN1 antibody. Bars = 25 μ m. Red arrowheads indicate the accumulation of PIN1 at lobe regions. D to I, Live images of GFP-tagged PIN1 (D–F) and PIN2 (G–I) in the roots. Bars = 50 μ m. White arrowheads indicate polarity of PIN localization. J, Quantitative analysis of PIN1 localization patterns in PCs. 1, PIN1 preferentially localized only to lobe sides. 2, PIN1 localized to lobe and indentation sides or nonlobing regions. 3, PIN1 localized to indentation sides. The percentage of three types of PIN1 localization patterns of PCs is shown on the right. K, Quantification of PIN1 and PIN2 polarity defects in the roots. The PIN localization pattern was quantified from more than 30 randomly chosen cells. WT, Wild type.

35S:TOPP4 PCs. 35S:PIN1-GFP was transiently expressed in wild-type, *topp4-1*, and 35S:TOPP4 PCs by the ballistics-mediated method (Fu et al., 2002). After treatment with 100 μM BFA, the plasma membrane-localized PIN1-GFP was rapidly internalized from the plasma membrane into BFA compartments in wild-type and 35S:TOPP4 PCs. However, in *topp4-1* PCs, intracellular accumulation of PIN1 was quite rare, with most PIN1-GFP remaining at the plasma membrane (Fig. 9A). Quantitative analysis showed that the frequency of cells with accumulated PIN1-GFP in BFA bodies was significantly lower in *topp4-1*, but higher in 35S:TOPP4 than in the wild type (Fig. 9B). This finding suggests that the BFA-induced PIN1 internalization is severely compromised in the *topp4-1* mutant, and TOPP4 overexpression in the wild type enhances BFA-induced PIN1 internalization.

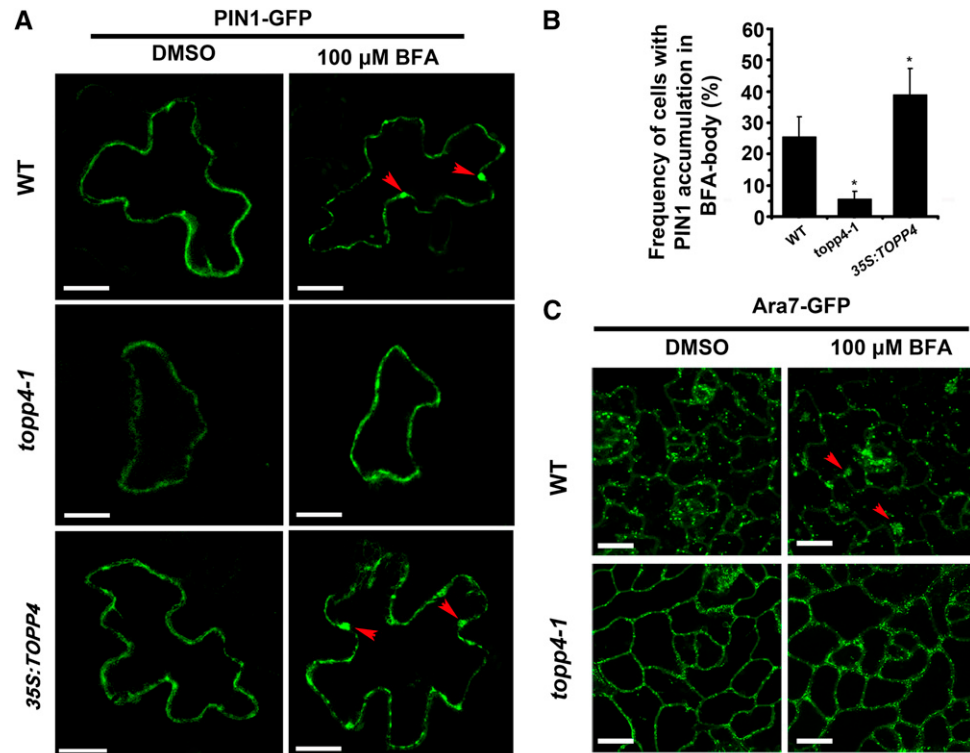
Next, we examined localization of the endocytic marker Ara7-GFP, which resides in an endosomal compartment and is necessary for targeting PIN1 to vacuoles or recycling to the plasma membrane (Lee et al., 2004). In wild-type PCs, Ara7-GFP was localized to endosomal compartments (Fig. 9C). After treatment with 100 μM BFA for 90 min, Ara7-GFP had accumulated greatly in intracellular endosomal aggregations (Fig. 9C). However, the localization of Ara7-GFP was affected in the *topp4-1* mutant by mainly residing in the plasma membrane (Fig. 9C). In addition, BFA-induced Ara7-GFP aggregations were rarely observed in *topp4-1* PCs (Fig. 9C). Taken together, these results suggest that TOPP4-mediated PIN1 dephosphorylation is required for

endocytic trafficking-dependent polar targeting of PIN1.

TOPP4 Is Involved in Regulation of ROP GTPase-Mediated Cytoskeletal Distribution

The reduced lobe expansion and narrow necks in the *topp4-1* mutant were similar to those in *rop2-1 rop4-1* and *ROP6-* or *RIC1*-overexpressing plants (Fu et al., 2002, 2005, 2009). To determine whether TOPP4 is required for the ROP GTPase-dependent auxin-signaling pathway, we first examined the expression of *ROP* genes in the *topp4-1* mutant by qRT-PCR. Compared with the wild type, *ROP2* and *ROP4* expression levels were lower, while the *ROP6* expression level was higher in *topp4-1* (Fig. 10A). Subsequently, we examined the effect of auxin on ROP2 activity in *topp4-1* stably expressing 35S:GFP-ROP2. Because RIC1 can specifically bind to the active-form ROP2 but not the inactive-form ROP2 both in vivo and in vitro, RIC1 has been used to measure ROP2 activity (Xu et al., 2010). Measurements of GFP-bound ROP2 showed that the activity of ROP2 was rapidly increased by auxin in wild-type plants (Fig. 10, B and C). However, auxin-stimulated ROP2 activity was abolished in the *topp4-1* mutant (Fig. 10, B and C). Furthermore, if TOPP4 positively regulates the activation of ROP2, the distributions of RIC1-GFP and RIC4-GFP should be disrupted in the *topp4-1* mutant. To verify this hypothesis, we first transiently expressed 35S:RIC1/ RIC4-GFP in the leaves of the wild-type plants and

Figure 9. PIN1-GFP and Ara7-GFP internalization in PCs after treatment with BFA. A, 35S:PIN1-GFP was transiently expressed for 24 h in leaf PCs, and then these leaves were treated with DMSO or 100 μM BFA. Red arrowheads represent the PIN1 accumulation in BFA bodies. Bars = 20 μm . B, Quantitative analyses of intracellular accumulation of PIN1 in BFA-treated PCs. Asterisks indicate significant difference from the wild type (WT; $P < 0.01$ by Student's *t* test). Error bars represent se ($n = 20$). C, Distribution of the endocytic marker Ara7-GFP in wild-type and *topp4-1* PCs. The leaves of wild-type and *topp4-1* plants labeled with Ara7-GFP treated with DMSO or 100 μM BFA. Red arrowheads represent the Ara7-GFP accumulation in BFA bodies. Bars = 50 μm .



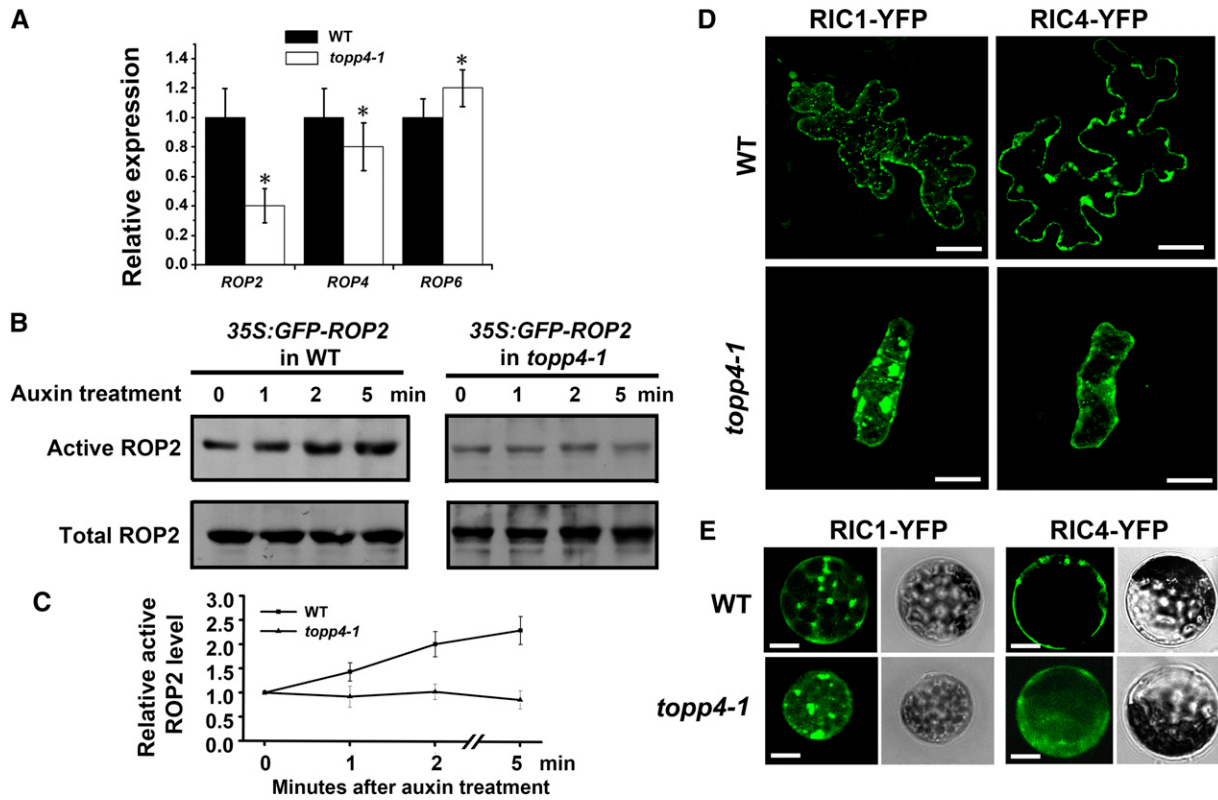


Figure 10. TOPP4 is required for the auxin-activated ROP-RIC pathway. **A**, The relative expression of *ROP2*, *ROP4*, and *ROP6* in *topp4-1*. Asterisks represent statistical differences from the wild type (WT) based on Student's *t* test with $P < 0.01$. **B**, Measurements of GTP-bound ROP2 activity in protoplasts isolated from the wild type and *topp4-1* stably expressing 35S:GFP-ROP2 by co-IP assay. **C**, Quantitative analyses of the relative active ROP2 activity. Error bars represent se ($n = 3$). **D**, The distribution patterns of RIC1-GFP and RIC4-GFP in the PCs of the wild type and *topp4-1*. Bars = 20 μ m. **E**, Transiently expressed RIC1-GFP and RIC4-GFP in protoplasts isolated from wild-type and *topp4-1* plants. Right section shows the bright field images of corresponding protoplasts. Scale bars = 20 μ m.

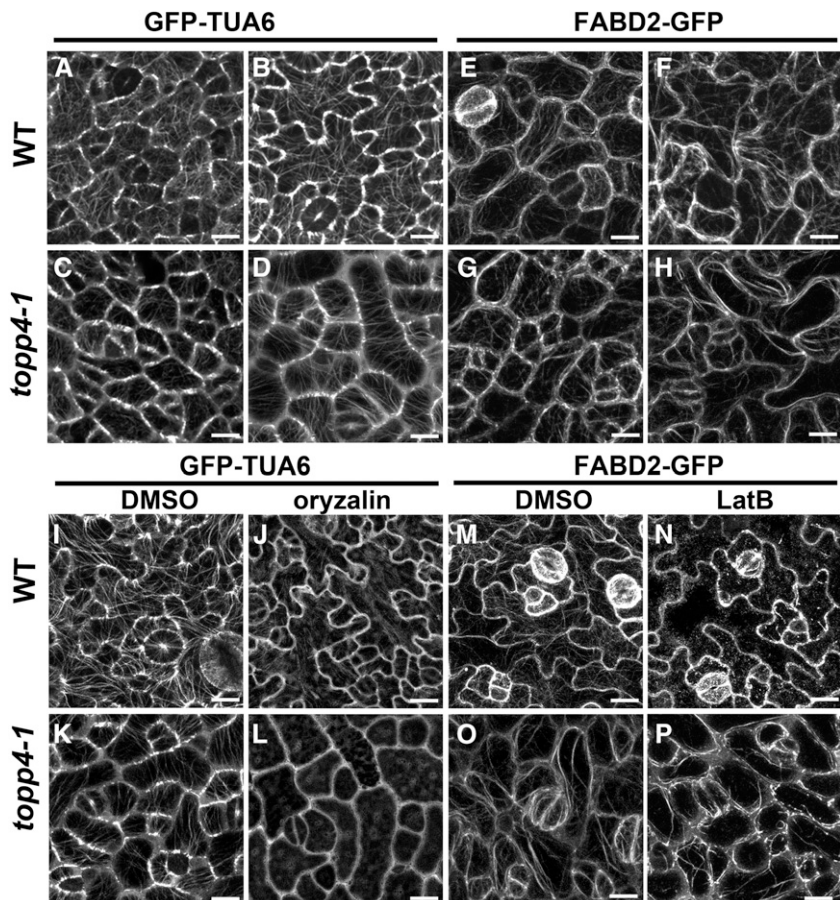
topp4-1 mutant by the ballistics-mediated method. In wild-type PCs, RIC1-GFP often formed numerous dot-like structures along cortical MTs. However, in *topp4-1* PCs, some RIC1-GFP had accumulated in very large structures (Fig. 10D). RIC4-GFP was preferentially localized to the lobe tips and plasma membrane of wild-type PCs (Fig. 10D), but its localization to the plasma membrane was replaced by diffuse distribution in the cytosols of *topp4-1* PCs (Fig. 10D). We also transiently expressed 35S:RIC1/RIC4-GFP in the protoplasts of the wild type and *topp4-1*. Similarly, we observed that the localization of RIC1-GFP and RIC4-GFP was compromised in *topp4-1* protoplasts (Fig. 10E). These results indicate that the ROP2 GTPase-dependent auxin-signaling pathway is disrupted in *topp4-1*.

Considering that the ROP-RIC pathway is defective in *topp4-1*, RIC1-associated cortical MTs and RIC4-associated F-actins may be disrupted in the mutant. We observed the cortical MT distribution in *topp4-1* PCs using GFP-tagged tubulin (Ueda et al., 1999). At the early development stage of PCs, cortical MTs were oriented randomly in both the wild type and *topp4-1*, but the number of MTs in *topp4-1* was lower than that of the

wild type (Fig. 11, A and C). At the late developmental stage of PCs, cortical MTs formed a fine and complex network with random orientations, and some transverse cortical MTs were present in the neck regions of the wild type (Fig. 11B). However, in *topp4-1*, the cortical MTs were highly ordered, and the MTs of most PCs were oriented perpendicularly to the long cellular axis (Fig. 11D). We also observed the actin distribution in *topp4-1* PCs using F-actins labeled with the second actin-binding domain of *Arabidopsis* fimbrin (FABD2; Voigt et al., 2005). At the early developmental stage of wild-type and *topp4-1* PCs, F-actins were found throughout the cell cortex, and strong fluorescence signals were associated with lobe formation sites (Fig. 11, E and G). At the late developmental stage of PCs, cortical F-actins had become more intense in the expanding lobes, and the F-actin cables formed a fine network in the wild type (Fig. 11F). Conversely, in *topp4-1*, cortical F-actin cables appeared to lose their fine network organization and formed some thicker actin cables along the plasma membrane of PCs (Fig. 11H).

To determine whether the observed MT disorganization in *topp4-1* was accompanied by changes in its stability, we

Figure 11. The organization of cortical MTs and F-actins is altered in *topp4-1*, and MTs are hypersensitive to oryzalin treatment, but F-actins are more resistant to LatB treatment in *topp4-1*. A to D, The cortical MT organization in PCs on the adaxial leaf side in wild-type (WT) and *topp4-1* plants labeled with GFP-Tubulin α -6 (TUA6). A and C, The early development stage of PCs. B and D, The late development stage of PCs. Bars = 25 μ m. E to H, The F-actin organization in PCs on the adaxial leaf side in the wild type and *topp4-1* labeled with FABD2-GFP. E and G, The early development stage of PCs. F and H, The late development stage of PCs. Bars = 25 μ m. I to L, The cortical MT organization in PCs in wild-type and *topp4-1* plants labeled with GFP-TUA6 treated with or without 20 μ M oryzalin for 45 min. Bars = 25 μ m. M to P, The F-actin organization in PCs in wild-type and *topp4-1* plants labeled with FABD2-GFP treated with or without 800 nM LatB for 30 min. Bars = 25 μ m.



compared the sensitivity of MTs to oryzalin (an MT-disrupting drug that disrupts MTs by binding to α -tubulin; Nakamura et al., 2004) in wild-type and *topp4-1* PCs. In *topp4-1* PCs, most MTs were completely disassembled after treatment with 20 μ M oryzalin for 45 min, while MTs in most wild-type PCs remained intact (Fig. 11, I–L). To assess the effect of TOPP4 on actin polymerization, we infiltrated wild-type and *topp4-1* seedlings with 800 nM latrunculin B (LatB) that inhibits actin polymerization by binding to monomeric actin and preventing its assembly on filament ends (Sampathkumar et al., 2011). After 30 min of LatB treatment, the F-actin bundles had disappeared completely and were replaced by diffuse green fluorescence in most wild-type PCs (Fig. 11, M and N). However, F-actin bundles remained largely in most of the *topp4-1* PCs (Fig. 11, O and P). These observations indicate that the *topp4-1* mutation enhances the sensitivity of MTs to oryzalin but reduces the sensitivity of F-actins to LatB in PCs. Taken together, these results suggest that TOPP4 affects PC cytoskeletal organization by coordinating MT stabilization and F-actin polymerization via the ROP GTPase-dependent auxin-signaling pathway.

DISCUSSION

Cell polarity and morphogenesis, which are critical for plant organ development, are modulated by numerous

cytoskeleton-associated proteins and various developmental and environmental signals (Fu et al., 2005; Hamant et al., 2008; Kleine-Vehn et al., 2008; Xu et al., 2010; Li et al., 2013). Cell polarity is often presented as a polar distribution of molecules within the cell. In Arabidopsis, the PIN family of auxin efflux carriers is asymmetrically targeted to the plasma membrane of cells, which is crucial for cell polarity and auxin distribution-dependent organogenesis (Benková et al., 2003). Previous studies indicate that the phosphorylation status of PIN proteins determine its polarity in embryos, inflorescences, and roots, mediated by PID, PP2A, and PP6 (Friml et al., 2004; Michniewicz et al., 2007; Kleine-Vehn et al., 2009; Dhonukshe et al., 2010; Huang et al., 2010; Dai et al., 2012). A recent study shows that PIN1 is polarly localized to the lobes of PCs, which is altered in a *fypp1* mutant (Xu et al., 2010; Li et al., 2011). Although it is known that phosphorylated PIN1 regulates PC interdigitation formation, how PIN1 is dephosphorylated in this process is still poorly understood. Here, we provide our extensive genetic and biochemical data to demonstrate that TOPP4 plays an antagonistic role with PID in regulating the polar localization and endocytosis of PIN1 in auxin-mediated PC morphogenesis via a reversible phosphorylation and dephosphorylation process (Fig. 12). We also found that TOPP4-dependent PIN1 dephosphorylation is involved in

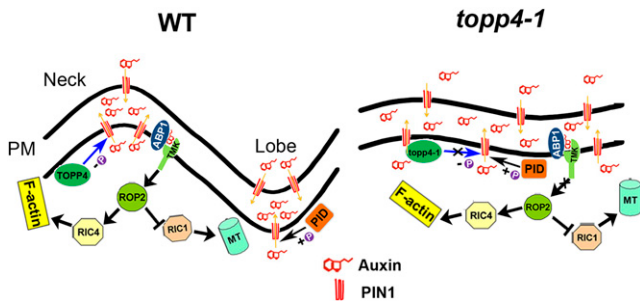


Figure 12. A current model for TOPP4 controlling interdigitated PC growth. In wild-type (WT) PCs, PIN kinase and TOPP4 phosphatase regulate PIN1 polarity in the lobes and indentations of PCs. The PIN1 polarity determines auxin flow and establishes auxin gradients in two adjacent PCs. This extracellular auxin in turn activates ROP GTPase signaling through the ABP1-TMK complex to control PC morphogenesis. By contrast, in *topp4-1* PCs, dephosphorylation of PIN1 is diminished, causing PIN1 to localize to indentation or nonlobing regions. Thus, the nonpolarity PIN1 reduces auxin accumulation in lobes and neighboring indentations of two adjacent PCs, disturbing the ROP GTPase signaling and causing the PC interdigitation defect (Pietra and Grebe, 2010; Chen and Yang, 2014). +P indicates phosphorylated status, and -P indicates dephosphorylated status. PM, Plasma membrane.

the coordination of ROP GTPase-mediated cytoskeletal distribution (Fig. 12).

A previous study showed that the PIN phosphorylation status, mediated by PID and PP2A, controls the polarity switch of PIN proteins by affecting their endocytic recycling in root cells (Geldner et al., 2001; Kleine-Vehn et al., 2009). In this study, our genetic analyses showed that TOPP4 functions antagonistically with PID in PIN1-mediated auxin promotion of PC interdigitation (Figs. 4 and 5). Biochemical analyses demonstrated that TOPP4 directly interacts with and dephosphorylates phosphorylated PIN1 protein in vitro and in vivo (Figs. 6 and 7). Further studies showed that the *topp4-1* mutation leads to alterations in PIN1 polarity (Fig. 8), which resembles the PIN1 polarity distribution of *fyp1* PCs and *35S:PID* or *pp2aa1 pp2aa3* root cells (Michniewicz et al., 2007; Li et al., 2011). It is well known that polar PIN localization is dynamic, and PIN proteins constitutively undergo cycles of exocytosis and endocytosis to and from the plasma membrane (Dhonukshe et al., 2007). Ara7-dependent endocytic trafficking is crucial for the generation of cell polarity in roots via regulating PIN polar localization (Tanaka et al., 2013). We showed that PIN1 dephosphorylation mediated by TOPP4 regulated its polar localization in PCs via affecting Ara7-dependent PIN1 internalization (Fig. 9C). The *topp4-1* mutation decreased BFA-induced PIN internalization in PCs, whereas *TOPP4* overexpression in the wild-type plants enhanced the sensitivity of PIN1 internalization to BFA (Fig. 9, A and B). These results are consistent with those from a previous report showing that *35S:PID* and *pp2aa1 pp2aa3* plants exhibit a reduction of BFA-induced PIN1 internalization in roots (Kleine-Vehn et al., 2009).

In addition, PIN1 endocytosis is increased in *dominant-negative mutant for ROP* and loss-of-function *rop4 R2i-34* mutants (Nagawa et al., 2012). In *topp4-1*, although the activity of ROP2 was reduced (Fig. 10), BFA-induced PIN1 internalization was inhibited (Fig. 9). These results suggest that the compromised localization of PIN1 in *topp4-1* PCs is not the effect of reduced ROP2 activity but rather due to the defect in PIN1 dephosphorylation caused by the *TOPP4* mutation, which is similar to the function of PP2A in roots (Kleine-Vehn et al., 2009).

Many studies have shown that MTs and F-actins play important roles in PC shape (Wang et al., 2007). It is well known that the ROP GTPase-signaling pathway regulates the organization of both cortical MTs and F-actins (Fu et al., 2002, 2005, 2009). Our results indicated that auxin-stimulated ROP2 activity was greatly disturbed in *topp4-1* (Fig. 10). Moreover, similar to *pin1* and *tmk* mutants (Xu et al., 2010, 2014), plasma membrane-localized RIC4-GFP was reduced and RIC1-GFP within cortical MTs was abolished in *topp4-1*, supporting a critical role of TOPP4 in localized ROP2 activation. The organization of RIC1-associated cortical MTs and RIC4-associated F-actins was also disrupted in *topp4-1* (Fig. 11), which is similar to that observed in *rop4 R2i* and *RIC1-OX* plants (Fu et al., 2005, 2009). Therefore, we concluded that TOPP4 is required for ROP GTPase-mediated cytoskeletal distribution in PCs.

Cell size is tightly correlated with its shape (Zhang et al., 2011). We found that the PC size of *topp4-1* was smaller than that of the wild type. To rule out the effect of cell size on cell shape, we analyzed auxin and ROP-RIC signaling and cytoskeleton organization in *cyclin D-type3;1* (*CYCD3;1*) overexpression plants, in which the PC size was also dramatically reduced compared with the wild type (Zhou et al., 2003; Supplemental Fig. S17). The circularity value of PCs in *35S:CYCD3;1* was similar to that of the wild type (Supplemental Fig. S17), indicating that the PC shape of *35S:CYCD3;1* was not altered. Furthermore, similar to wild-type plants, auxin and ROP-RIC signaling were normal in *35S:CYCD3;1* plants (Supplemental Fig. S18). The cortical MTs and F-actins also showed normal distribution in *35S:CYCD3;1* PCs compared with wild-type PCs (Supplemental Fig. S18). These results suggest that the abnormal PC shape in *topp4-1* is not caused by the small cell size effects on auxin signaling.

PIN1-mediated auxin efflux may lead to a localized accumulation of extracellular auxin in the indenting region of neighboring cells, activating complementary ROP2 and ROP6 pathways in two adjacent cells through a cell surface auxin perception complex, ABP1-TMK (Xu et al., 2010, 2014; Li et al., 2011). Therefore, based on the aforementioned results, we propose that the ROP GTPase signaling may be at the downstream of TOPP4. In wild-type PCs, hypophosphorylated PIN1, mediated by TOPP4, localizes preferentially to the plasma membrane of lobe regions, promoting the auxin flow from lobes to neighboring indentations and forming a localized accumulation of extracellular auxin in two adjacent cells. This extracellular auxin in turn activates ROP signaling via its perception complex to control PC

morphogenesis by regulating the organization of cortical MTs and F-actins. In *topp4-1* PCs, dephosphorylation of PIN1 is abolished, causing hyperphosphorylated PIN1 to localize to indentation or nonlobing regions. This non-polarity of PIN1 distribution reduces auxin accumulation in lobes and neighboring indentations, thus inactivating ROP2 and disturbing RIC-controlled cytoskeletal organization, resulting in abnormal PCs. In addition, as the PC defects in *topp4-1* were more severe than those in auxin transport-defective mutants, such as *pin1* and *35S:PID* (Fig. 4), we could not completely exclude the possibility that TOPP4 also participates in another pathway to regulate PC morphogenesis.

The mechanism of TOPP4 in PP1 family modulating the PIN1 phosphorylation status is similar to the action of PP2A and PP6 (Michniewicz et al., 2007; Dai et al., 2012). The catalytic domains of Ser/Thr-specific phosphoprotein phosphatases are highly conserved among all eukaryotes (Farkas et al., 2007; Shi, 2009). As a catalytic subunit of protein phosphatase, TOPP4 must bind to different regulatory subunits to form a functional enzyme to participate in multiple signaling pathways (Tian and Wang, 2002). Because the regulatory subunits of phosphatases are dynamic at different developmental stages or in response to various environmental signals (Dai et al., 2013), PP1 and PP6 may respond to different developmental signals in different organs or tissues at various developmental stages. The *topp4-1* mutant showed PC defects only in and after the third true leaves, whereas the *fypp1* mutant has PC defects in cotyledons and true leaves (Li et al., 2011). Furthermore, TOPP4 was only detected in the stele cells of the root, but *FyPP1* and *FyPP3* were ubiquitously expressed in the root. Therefore, the root defect in the *fypp* mutant was more severe than that in *topp4-1* (Dai et al., 2012). Thus, although PP1 and PP6 share similar substrates and catalytic action, they may perform different functions in different developmental organs and tissues through binding to specific regulatory subunits. Future investigation will focus on identifying the different regulatory subunits of TOPP4.

MATERIALS AND METHODS

Plant Materials and Growth Conditions

Plants were grown on either one-half-strength Murashige and Skoog (MS) medium or soil in greenhouse at 22°C ± 1°C, with a 16-h-light/8-h-dark photoperiod. The double mutants *topp4-1 pin1*, *topp4-1 35S:PID*, and *topp4-1 pid-3* were generated from the separate crosses of *topp4-1* with *pin1* (SALK_047613, from the Arabidopsis Biological Resource Center), *35S:PID* 21# (N9867, from the European Arabidopsis Stock Centre [NASC]), and *pid-3* (N5219, from NASC), respectively. Double mutants were identified from the F2 progeny by PCR-based molecular analyses. Primers used for identifying homozygous lines are indicated in Supplemental Table S1. The *topp4-1* crossed with DR5:GUS, DR5:GFP, PIN1-GFP (N23889, from NASC), or Ara7-GFP (Lee et al., 2004) lines and screened the homozygous lines from the F2 progeny by PCR-based analysis and GFP fluorescence observation.

Plasmid Construction

For transient expression in *Arabidopsis* (*Arabidopsis thaliana*) leaves or protoplasts, full-length complementary DNAs of *PIN1*, *RIC1*, and *RIC4* were

amplified and cloned into pA7-GFP vector. Primers used for plasmid construction are indicated in Supplemental Table S1.

Microscopic Analyses of PC Shape

The third true leaves from 21-d-old seedlings were used for phenotype analyses. The *Arabidopsis* leaves were stained with 10 μM FM4-64 dye (Sigma) for 30 min and imaged using a confocal microscopy (Olympus Fluoview FV1000MPE). Both lobe length and neck width were measured with Image J, as described by Fu et al. (2002). The measurements were consistently conducted on PCs at the same developmental stage. Each piece of data was averaged from the measurements of 100 cells of five leaves. Data from different figures were obtained from independent experiments.

Chemical Treatments

To detect the effects of tautomycin (Merck) on the PC morphology, the seeds were grown on one-half-strength MS agar plates that were supplemented with 0.1 or 1 μM tautomycin. To examine the effect of exogenous auxin on the degree of PC interdigitation, NAA or IAA (Sigma) was dissolved in dimethyl sulfoxide (DMSO) and prepared as a stock solution of 100 μM, which was added into one-half-strength MS media to obtain a final concentration of 20 nm NAA or 100 nm IAA for seedling treatments. Analysis of PIN1-GFP internalization was performed as described by Nagawa et al. (2012). *35S:PIN1-GFP* was transiently transfected in *Arabidopsis* leaves for 24 h by ballistics-mediated method, and then these leaves were treated with DMSO or 100 μM BFA for 90 min. PIN1-GFP signal was observed by the confocal microscopy. Each treatment was repeated at least three times with three independent seedlings each time.

Visualization of F-Actins and MTs and Drug Treatments

To visualize the cortical MTs and F-actins in leaf PCs, we crossed GFP-tagged α-tubulin (Ueda et al., 1999) or FABD2-GFP (Voigt et al., 2005) into *topp4-1* and examined their distribution using the confocal microscope. For oryzalin (Sigma) treatments, 21-d-old seedlings expressing GFP-tagged α-tubulin were incubated in one-half-strength MS medium containing DMSO or 20 μM oryzalin for 45 min. For LatB (Sigma) treatments, 21-d-old seedlings expressing FABD2-GFP were incubated with one-half-strength MS medium containing DMSO or 800 nm LatB for 30 min. Each treatment was repeated at least three times.

Yeast Two-Hybrid Assay

The yeast (*Saccharomyces cerevisiae*) strain Y190 was used in our experiments. Yeast transformations were performed according to the MATCH-MAKER two-hybrid system 3 (Clontech). Full-length *TOPP4* gene fused to the DNA-binding domain of GAL4 was used as the bait protein, and *PIN1HL* fused to the transcriptional activation domain of GAL4 was used as the prey protein. Yeast clones containing the *GAL4-BD-TOPP4* and *GAL4-AD-PIN1HL* constructs were plated on SD-His-Trp-Leu medium for 5 d at 30°C to assay for interaction. β-gal activity was performed according to the manufacturer's protocol (Clontech). This experiment was repeated at least three times.

In Vitro Pull-Down and co-IP Assays

The GST-TOPP4 and HIS-PIN1HL proteins were expressed in *Escherichia coli* BL21. The recombinant proteins were coincubated in the presence of glutathione Sepharose 4B resin (GE), which was used to selectively bind the GST fusion proteins with phosphate-buffered saline (PBS) buffer (140 mM NaCl, 2.7 mM KCl, 10 mM Na₂HPO₄, and 1.8 mM KH₂PO₄). The bound proteins were eluted with 1× SDS loading buffer and analyzed with anti-GST and anti-HIS antibodies. This experiment was repeated at least three times.

co-IP studies of TOPP4 and PIN1 were performed on 10-d-old seedlings of *35S:TOPP4 PIN1:PIN1-GFP* and *35S:TOPP4*. IP of PIN1 protein used an anti-GFP antibody (Invitrogen). Protein G agarose (GE) was used to precipitate the immunoprotein complexes with IP buffer (50 mM Tris-HCl, pH 7.5, 150 mM NaCl, 5 mM EDTA, 0.2% [v/v] Triton X-100, and 1% [v/v] protease inhibitors). After IP, beads were washed four times with IP buffer. Proteins were then released and collected by boiling in 2× SDS loading buffer for 5 min.

IP products were detected by immunoblot analysis with a TOPP4 antibody. This experiment was repeated at least three times.

BiFC Assay

The coding sequence of sequences of TOPP4 or *PIN1* was amplified and cloned into pEarleygate201-YN or pEarleygate202-YC BiFC vectors to generate TOPP4-N-terminal yellow fluorescent protein or PIN1-C-terminal yellow fluorescent protein, respectively (Song et al., 2010). *Agrobacterium tumefaciens* strains containing the BiFC constructs and the p19-silencing plasmid were infiltrated into leaves of 4-week-old *Nicotiana benthamiana* plants (Feng et al., 2008). The YFP fluorescence was observed with confocal laser-scanning microscopy.

Immunofluorescence Microscopy

Whole-mount immunolocalization on Arabidopsis leaf PCs were performed as described (Sauer et al., 2006; Li et al., 2011). Briefly, true leaves were submerged into a fixation solution (PBS plus 4% paraformaldehyde) for 1 h. Fixed leaves were washed in PBS two to three times for 5 to 10 min each. PBS was removed, pure methanol was added, and materials were incubated for 10 min at 37°C; this was repeated two more times until chlorophyll was gone. The materials were transferred to wash buffer (1× PBS and 50 mM Gly) in Eppendorf tubes, and 3% bovine serum albumin was added for 1 h. The materials were incubated with a PIN1 antibody (NASC, 1:200) at 37°C for 3 h and then incubated with a second antibody (fluorescein isothiocyanate-conjugated anti-sheep IgG [1:200], KPL) for 1 to 3 h at 37°C. Stained tissues were observed under confocal microscope. Lobe and indentation regions containing PIN1 were quantified from over 30 cells from three independent experiments. Preferential localization of PIN1 to lobes or indentations and equal localization to both regions were determined by eyeballing of the confocal stacked images.

Antibodies and IP Assay

Anti-TOPP4 polyclonal antibodies were raised against the N terminus of TOPP4 (amino acids 1–150), which is specific for TOPP4 protein, in rabbits. Antiserum was isolated from rabbits immunized alternately with soluble recombinant HIS-TOPP4 N150aa protein. One-half gram of cyanogen bromide-activated Sepharose 4B (GE Healthcare) was incubated with 20 mg of HIS-TOPP4 N150aa for 1 h; the medium was transferred to 0.1 M Tris-HCl, pH 8.0, for 2 h and washed alternatively with 0.5 M NaCl, 0.1 M ethanoic acid, pH 4.0, 0.5 M NaCl, and 0.1 M Tris-HCl, pH 8.0; the Sepharose was balanced, mixed with antiserum slowly for 40 min, and washed with buffer (0.1 M citric acid, pH 2.0); and the anti-TOPP4 polyclonal antibodies were eluted with elution buffer (1 M Tris-HCl, pH 8.0).

For IP assay, 21-d-old seedlings were harvested and suspended in IP buffer (20 mM HEPES, pH 7.5, 40 mM KCl, 1 mM dithiothreitol [DTT], and 1% protease inhibitors [Sigma-Aldrich]). TOPP4 or *topp4-1* was immunoprecipitated from wild-type or *topp4-1* plants using the anti-TOPP4 antibody followed by protein A beads. The beads in column were washed by IP buffer containing 0.2% Triton X-100 three times. After IP, the beads were suspended in 50 μL of IP buffer containing 1% of the protease inhibitor cocktail. Immunoprecipitated proteins were detected by immunoblot analysis with the anti-TOPP4 at 1:400 dilutions.

In Vitro Phosphorylation Assays

Arabidopsis protoplasts were isolated from leaves of 4-week-old plants, transformed according to Meskiene et al. (2003) and harvested after 10 to 22 h. Cell pellets were lysed by freeze-thaw cycles followed by a Dounce-type homogenizer. The extraction buffer used was previously described (Michniewicz et al., 2007; Abas and Luschnig, 2010).

Membrane fractions were solubilized with 0.1% Brij35 (Sigma) and preheated at 65°C for 10 min to inactivate endogenous enzymes. After λ-phosphatase buffer (New England Labs) was added, four treatments were performed in a final volume of 30 mL: sample plus 3 mM MnCl₂; sample plus 3 mM MnCl₂ and 100 units of λ-phosphatase (New England Labs); and sample plus TOPP4 or *topp4-1*, which was immunoprecipitated with anti-TOPP4 antibody from wild-type or *topp4-1* plants, respectively. All samples were incubated at 30°C for 30 min. These experiments were repeated at least three times.

Recombinant HIS-tagged PIN1 hydrophilic loop (HIS-PIN1HL) was expressed in *E. coli* and purified using N'-nitrotriacetic acid resin (Invitrogen).

Total proteins were extracted with 1× kinase buffer (25 mM Tris-HCl, pH 7.5, 1 mM DTT, and 5 mM MgCl₂) plus 1× protease inhibitor and 1 mM phenylmethylsulfonyl fluoride. According to previous methods (Michniewicz et al., 2007; Dhonukhsa et al., 2010; Dai et al., 2012), 1 μg of HIS-PIN1HL and 25 μg of plant seedling extracts were mixed in 1× kinase buffer and 1× ATP solution (100 μM ATP and 1 μCi [γ -³²P] ATP) in a total volume of 25 μL. The reactions were incubated at 30°C for 30 min and then stopped by adding 5× loading buffer and boiling for 5 min, or approximately 1 μg of purified HIS-PIN1HL was phosphorylated by GST-PID using kinase reaction mix and then incubated at 30°C for 3 h with TOPP4, *topp4-1*, or denatured TOPP4, which were immunoprecipitated from the wild type or *topp4-1*. Products were separated by electrophoresis through 12.5% acrylamide gels, and the gels were stained, dried, and then visualized by exposure to x-ray films.

In Vivo Phosphorylation Assays

Arabidopsis seedlings expressing *PIN1:PIN1-GFP* in wild-type, *topp4-1*, and *35S:TOPP4* backgrounds were grown to 12 d, and then these seedlings were harvested. The membrane protein extraction was performed as previously described (Michniewicz et al., 2007; Abas and Luschnig, 2010). PIN1-GFP was immunoprecipitated by incubation with anti-GFP antibody-coupled protein A beads. Membrane fractions were subjected to λ-phosphatase treatment as described previously (Dai et al., 2012). Samples were separated as described (Abas and Luschnig, 2010) and probed with the anti-GFP antibody (1:1,000; Invitrogen).

Particle Bombardment-Mediated Transient Expression in Arabidopsis Leaves

For particle bombardment, all plasmids were amplified in *E. coli* strain DH5α and purified using plasmid midi or mini kits according to the manufacturer's instructions (Qiagen). Expanding rosette leaves of 0.8 to 1.2 cm in length were collected from 3-week-old plants and were bombarded with gold particles coated with plasmids using a Bio-Rad PDS-1000/He particle delivery system. In all experiments, 0.5 g of constructs were used. The bombardment procedure was described previously for leaves (Fu et al., 2002). Bombarded leaves were incubated in water before observation with the confocal microscope.

ROP2 Activity Assay

GFP-tagged active ROP2 was pulled down by use of GST-RIC1 as described previously (Xu et al., 2010). Arabidopsis protoplasts were isolated from leaves of 3-week-old wild-type or *topp4-1* plants transformed with *35S:GFP-ROP2* and harvested after 4 to 6 h. The protoplasts were treated with or without 100 nM NAA and frozen by liquid nitrogen. Total protein was extracted from 10⁵ to 10⁶ protoplasts by extraction buffer (25 mM HEPES, pH 7.4, 10 mM MgCl₂, 10 mM KCl, 5 mM DTT, 5 mM Na₃VO₄, 5 mM NaF, 1 mM phenylmethylsulfonyl fluoride, 1% protease inhibitor, and 1% TritonX-100). A part of total proteins was used as control to determine the total amount of GFP-ROP2. A saturated amount of GST-RIC1-conjugated beads was added to the same amount of protoplast extracts, which were then gently shaken at 4°C for 2 h. Beads were washed in a washing buffer (25 mM HEPES, pH 7.4, 1 mM EDTA, 5 mM MgCl₂, 1 mM DTT, and 0.5% TritonX-100) for three times at 4°C (5 min each). Western blotting with the anti-GFP antibody was used for analysis of the GTP-bound active form of GFP-ROP2 that was associated with the GST-RIC1 beads.

Sequence data from this article can be found in the GenBank/EMBL data libraries under accession numbers *TOPP4* (At2g39840), *PIN1* (AT1G73590), *PID* (AT2G34650), *ROP2* (AT1G20090), *ROP4* (AT1G75840), *ROP6* (AT4G35020), *RIC1* (AT2G33460), and *RIC4* (AT5G16490).

Supplemental Data

The following supplemental materials are available.

Supplemental Figure S1. Tissue-specific expression of TOPP4 protein.

Supplemental Figure S2. The rosette leaf phenotypes of *topp4-1*.

Supplemental Figure S3. The cotyledon PCs show normal shape in *topp4-1*.

Supplemental Figure S4. Effect of TOPP4 mutation on PC development at different stages.

Supplemental Figure S5. Transformed *TOPP4:TOPP4* into the *topp4-1* mutant slightly rescues the mutant phenotype.

Supplemental Figure S6. Phenotype analysis of two transfer DNA insertion alleles of *TOPP4*.

Supplemental Figure S7. The *TOPP4/topp4-1* expression levels of the 35S: *TOPP4*, *TOPP4:topp4-1-GFP*, or 35S:*topp4-1-GFP* transgenic plants.

Supplemental Figure S8. Inhibition of PP1 partially repressed interdigitated growth of PCs.

Supplemental Figure S9. The *topp4-1* mutant shows auxin-related defects.

Supplemental Figure S10. The phenotype of *topp4-1 pin1* double mutants.

Supplemental Figure S11. Effect of tautomycin on PC shape in wild-type, *pin1*, 35S:*PID*, and *pid-3* plants.

Supplemental Figure S12. The phenotype of *topp4-1 35S:PID* double mutants.

Supplemental Figure S13. The phenotype of 2-month-old *topp4-1 pid-3* double mutants.

Supplemental Figure S14. Transient expression of 35S:*PIN1-GFP* and 35S: *PID-FLAG* in Arabidopsis protoplasts.

Supplemental Figure S15. Immunoblot analyses of *PIN1-GFP* in wild-type, *topp4-1*, and 35S:*TOPP4* plants expressing *PIN1:PIN1-GFP*.

Supplemental Figure S16. PIN1 internalization in root cells after BFA treatment.

Supplemental Figure S17. The effect of exogenous auxin on the PC lobe formation in 35S:*CYCD3;1*.

Supplemental Figure S18. The effect of auxin on ROP2 activity and the organization of cortical MTs and F-actins in 35S:*CYCD3;1*.

Supplemental Table S1. Primers used for plasmid construction and qRT-PCR.

ACKNOWLEDGMENTS

We thank Xiaoping Gou, Yun Xiang, Longfeng Yan, and Qingxiang Gao for technical assistance, Yun Xiang for providing FABD2-GFP seeds, Verónica A. Grieneisen (Utrecht University) for providing Ara7-GFP seeds, and Yongming Zhou (Huazhong University) for providing 35S:*CYCD3;1* seeds.

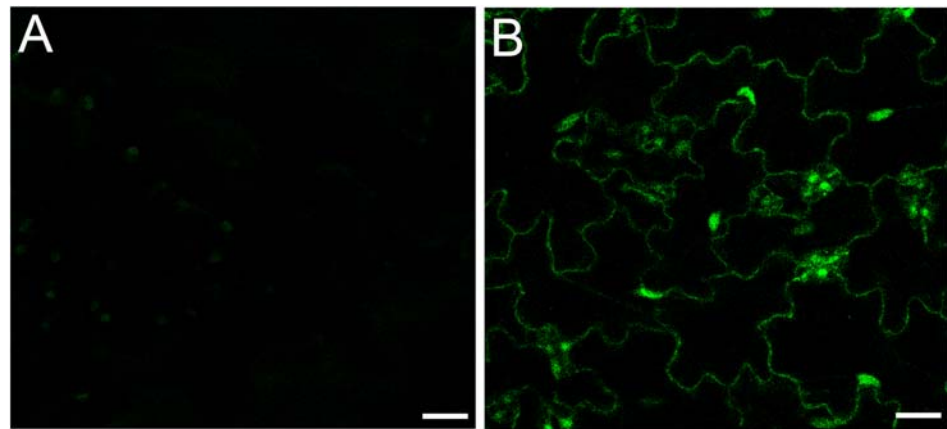
Received September 5, 2014; accepted December 31, 2014; published January 5, 2015.

LITERATURE CITED

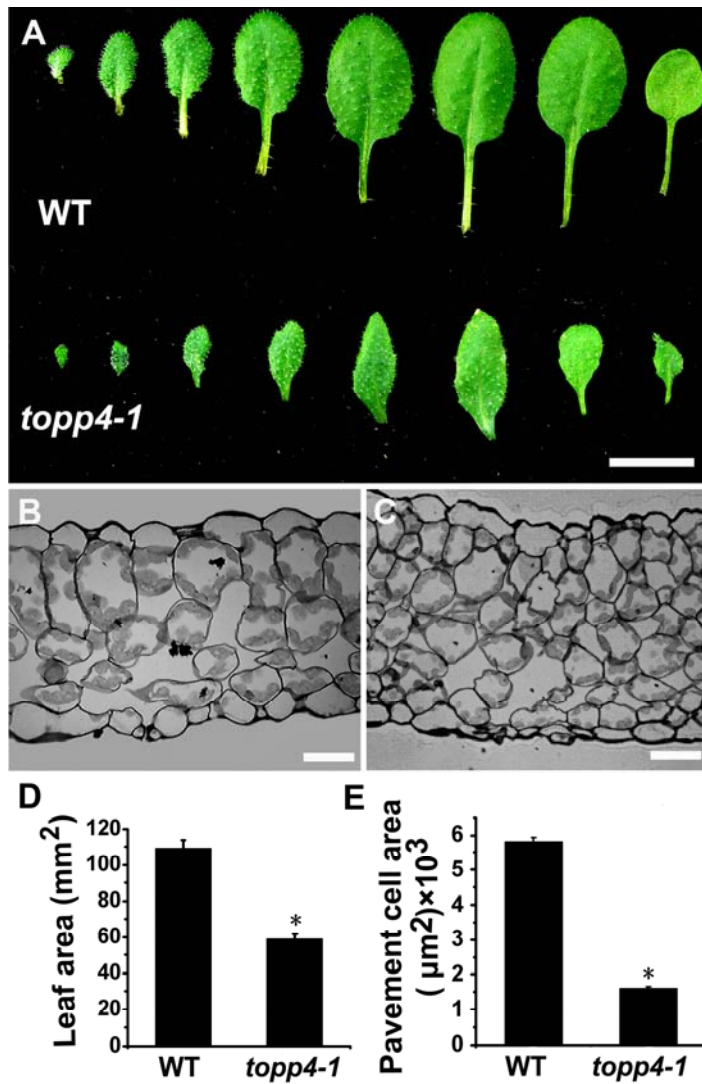
- Abas L, Luschnig C (2010) Maximum yields of microsomal-type membranes from small amounts of plant material without requiring ultracentrifugation. *Anal Biochem* 401: 217–227
- Benjamins R, Quint A, Weijers D, Hooykaas P, Offringa R (2001) The PINOID protein kinase regulates organ development in Arabidopsis by enhancing polar auxin transport. *Development* 128: 4057–4067
- Benková E, Michniewicz M, Sauer M, Teichmann T, Seifertová D, Jürgens G, Friml J (2003) Local, efflux-dependent auxin gradients as a common module for plant organ formation. *Cell* 115: 591–602
- Bilou I, Xu J, Wildwater M, Willemsen V, Paponov I, Friml J, Heidstra R, Aida M, Palme K, Scheres B (2005) The PIN auxin efflux facilitator network controls growth and patterning in Arabidopsis roots. *Nature* 433: 39–44
- Chary SN, Hicks GR, Choi YG, Carter D, Raikhel NV (2008) Trehalose-6-phosphate synthase/phosphatase regulates cell shape and plant architecture in Arabidopsis. *Plant Physiol* 146: 97–107
- Chen J, Yang Z (2014) Novel ABP1-TMK auxin sensing system controls ROP GTPase-mediated interdigitated cell expansion in Arabidopsis. *Small GTPases* 30: e29711
- Dai M, Terzaghi W, Wang H (2013) Multifaceted roles of Arabidopsis PP6 phosphatase in regulating cellular signaling and plant development. *Plant Signal Behav* 8: e22508
- Dai M, Zhang C, Kania U, Chen F, Xue Q, McCray T, Li G, Qin G, Wakeley M, Terzaghi W, et al (2012) A PP6-type phosphatase holoenzyme directly regulates PIN phosphorylation and auxin efflux in *Arabidopsis*. *Plant Cell* 24: 2497–2514
- Dewitte W, Riou-Khamlichi C, Scofield S, Healy JM, Jacqmard A, Kilby NJ, Murray JA (2003) Altered cell cycle distribution, hyperplasia, and inhibited differentiation in Arabidopsis caused by the D-type cyclin CYCD3. *Plant Cell* 15: 79–92
- Dhonukshe P, Aniento F, Hwang I, Robinson DG, Mravec J, Stierhof YD, Friml J (2007) Clathrin-mediated constitutive endocytosis of PIN auxin efflux carriers in Arabidopsis. *Curr Biol* 17: 520–527
- Dhonukshe P, Huang F, Galvan-Ampudia CS, Mähönen AP, Kleine-Vehn J, Xu J, Quint A, Prasad K, Friml J, Scheres B, et al (2010) Plasma membrane-bound AGC3 kinases phosphorylate PIN auxin carriers at TPRXS(N/S) motifs to direct apical PIN recycling. *Development* 137: 3245–3255
- Falbel TG, Koch LM, Nadeau JA, Segui-Simarro JM, Sack FD, Bednarek SY (2003) SCD1 is required for cytokinesis and polarized cell expansion in *Arabidopsis thaliana* [corrected]. *Development* 130: 4011–4024
- Farkas I, Dombrádi V, Miskei M, Szabados L, Koncz C (2007) Arabidopsis PPP family of serine/threonine phosphatases. *Trends Plant Sci* 12: 169–176
- Favre B, Turowski P, Hemmings BA (1997) Differential inhibition and posttranslational modification of protein phosphatase 1 and 2A in MCF7 cells treated with calyculin-A, okadaic acid, and tautomycin. *J Biol Chem* 272: 13856–13863
- Friml J, Yang X, Michniewicz M, Weijers D, Quint A, Tietz O, Benjamins R, Ouwerkerk PB, Ljung K, Sandberg G, et al (2004) A PINOID-dependent binary switch in apical-basal PIN polar targeting directs auxin efflux. *Science* 306: 862–865
- Fu Y, Gu Y, Zheng Z, Wasteneys G, Yang Z (2005) Arabidopsis interdigitating cell growth requires two antagonistic pathways with opposing action on cell morphogenesis. *Cell* 120: 687–700
- Fu Y, Li H, Yang Z (2002) The ROP GTPase controls the formation of cortical fine F-actin and the early phase of directional cell expansion during *Arabidopsis* organogenesis. *Plant Cell* 14: 777–794
- Fu Y, Xu T, Zhu L, Wen M, Yang Z (2009) A ROP GTPase signaling pathway controls cortical microtubule ordering and cell expansion in Arabidopsis. *Curr Biol* 19: 1827–1832
- Gälweiler L, Guan C, Müller A, Wisman E, Mendgen K, Yephremov A, Palme K (1998) Regulation of polar auxin transport by AtPIN1 in Arabidopsis vascular tissue. *Science* 282: 2226–2230
- Geldner N, Friml J, Stierhof YD, Jürgens G, Palme K (2001) Auxin transport inhibitors block PIN1 cycling and vesicle trafficking. *Nature* 413: 425–428
- Guo X, Lu W, Ma Y, Qin Q, Hou S (2013) The *BIG* gene is required for auxin-mediated organ growth in Arabidopsis. *Planta* 237: 1135–1147
- Hamant O, Heisler MG, Jönsson H, Krupinski P, Uyttewaal M, Bokov P, Corson F, Sahlin P, Boudaoud A, Meyerowitz EM, et al (2008) Developmental patterning by mechanical signals in Arabidopsis. *Science* 322: 1650–1655
- Huang F, Zago MK, Abas L, van Marion A, Galván-Ampudia CS, Offringa R (2010) Phosphorylation of conserved PIN motifs directs *Arabidopsis* PIN1 polarity and auxin transport. *Plant Cell* 22: 1129–1142
- Kleine-Vehn J, Dhonukshe P, Sauer M, Brewer PB, Wiśniewska J, Paciorek T, Benková E, Friml J (2008) ARF GEF-dependent transcytosis and polar delivery of PIN auxin carriers in Arabidopsis. *Curr Biol* 18: 526–531
- Kleine-Vehn J, Huang F, Naramoto S, Zhang J, Michniewicz M, Offringa R, Friml J (2009) PIN auxin efflux carrier polarity is regulated by PINOID kinase-mediated recruitment into GNOM-independent trafficking in *Arabidopsis*. *Plant Cell* 21: 3839–3849
- Lee GJ, Sohn EJ, Lee MH, Hwang I (2004) The Arabidopsis rab5 homologs rha1 and ara7 localize to the prevacuolar compartment. *Plant Cell Physiol* 45: 1211–1220
- Li H, Lin D, Dhonukshe P, Nagawa S, Chen D, Friml J, Scheres B, Guo H, Yang Z (2011) Phosphorylation switch modulates the interdigitated pattern of PIN1 localization and cell expansion in Arabidopsis leaf epidermis. *Cell Res* 21: 970–978
- Li H, Xu T, Lin D, Wen M, Xie M, Duclercq J, Bielach A, Kim J, Reddy GV, Zuo J, et al (2013) Cytokinin signaling regulates pavement cell morphogenesis in Arabidopsis. *Cell Res* 23: 290–299
- Lin D, Cao L, Zhou Z, Zhu L, Ehrhardt D, Yang Z, Fu Y (2013) Rho GTPase signaling activates microtubule severing to promote microtubule ordering in Arabidopsis. *Curr Biol* 23: 290–297

- Lin Q, Li J, Smith RD, Walker JC** (1998) Molecular cloning and chromosomal mapping of type one serine/threonine protein phosphatases in *Arabidopsis thaliana*. *Plant Mol Biol* **37**: 471–481
- Mathur J, Mathur N, Kernebeck B, Hülskamp M** (2003) Mutations in actin-related proteins 2 and 3 affect cell shape development in *Arabidopsis*. *Plant Cell* **15**: 1632–1645
- Meskiene I, Baudouin E, Schweighofer A, Liwosz A, Jonak C, Rodriguez PL, Jelinek H, Hirt H** (2003) Stress-induced protein phosphatase 2C is a negative regulator of a mitogen-activated protein kinase. *J Biol Chem* **278**: 18945–18952
- Michniewicz M, Zago MK, Abas L, Weijers D, Schweighofer A, Meskiene I, Heisler MG, Ohno C, Zhang J, Huang F, et al** (2007) Antagonistic regulation of PIN phosphorylation by PP2A and PINOID directs auxin flux. *Cell* **130**: 1044–1056
- Nagawa S, Xu T, Lin D, Dhonukshe P, Zhang X, Friml J, Scheres B, Fu Y, Yang Z** (2012) ROP GTPase-dependent actin microfilaments promote PIN1 polarization by localized inhibition of clathrin-dependent endocytosis. *PLoS Biol* **10**: e1001299
- Nakamura M, Naoi K, Shoji T, Hashimoto T** (2004) Low concentrations of propyzamide and oryzalin alter microtubule dynamics in *Arabidopsis* epidermal cells. *Plant Cell Physiol* **45**: 1330–1334
- Petrásek J, Mravec J, Bouchard R, Blakeslee JJ, Abas M, Seifertová D, Wisniewska J, Tadele Z, Kubas M, Cováňová M, et al** (2006) PIN proteins perform a rate-limiting function in cellular auxin efflux. *Science* **312**: 914–918
- Pietra S, Grebe M** (2010) Auxin paves the way for planar morphogenesis. *Cell* **143**: 29–31
- Qian P, Hou S, Guo G** (2009) Molecular mechanisms controlling pavement cell shape in *Arabidopsis* leaves. *Plant Cell Rep* **28**: 1147–1157
- Qin Q, Wang W, Guo X, Yue J, Huang Y, Xu X, Li J, Hou S** (2014) *Arabidopsis* DELLA protein degradation is controlled by a type-one protein phosphatase, TOPP4. *PLoS Genet* **10**: e1004464
- Sampathkumar A, Lindeboom JJ, Debolt S, Gutierrez R, Ehrhardt DW, Ketelaars T, Persson S** (2011) Live cell imaging reveals structural associations between the actin and microtubule cytoskeleton in *Arabidopsis*. *Plant Cell* **23**: 2302–2313
- Sauer M, Paciorek T, Benková E, Friml J** (2006) Immunocytochemical techniques for whole-mount *in situ* protein localization in plants. *Nat Protoc* **1**: 98–103
- Shi Y** (2009) Serine/threonine phosphatases: mechanism through structure. *Cell* **139**: 468–484
- Smith RD, Walker JC** (1993) Expression of multiple type 1 phosphoprotein phosphatases in *Arabidopsis thaliana*. *Plant Mol Biol* **21**: 307–316
- Song Y, Wu K, Dhaubhadel S, An L, Tian L** (2010) *Arabidopsis* DNA methyltransferase AtDNMT2 associates with histone deacetylase AtHD2s activity. *Biochem Biophys Res Commun* **396**: 187–192
- Stubbs MD, Tran HT, Atwell AJ, Smith CS, Olson D, Moorhead GB** (2001) Purification and properties of *Arabidopsis thaliana* type 1 protein phosphatase (PP1). *Biochim Biophys Acta* **1550**: 52–63
- Takemiya A, Kinoshita T, Asanuma M, Shimazaki K** (2006) Protein phosphatase 1 positively regulates stomatal opening in response to blue light in *Vicia faba*. *Proc Natl Acad Sci USA* **103**: 13549–13554
- Tanaka H, Kitakura S, Rakusová H, Uemura T, Feraru MI, De Rycke R, Robert S, Kakimoto T, Friml J** (2013) Cell polarity and patterning by PIN trafficking through early endosomal compartments in *Arabidopsis thaliana*. *PLoS Genet* **9**: e1003540
- Tian Q, Wang J** (2002) Role of serine/threonine protein phosphatase in Alzheimer's disease. *Neurosignals* **11**: 262–269
- Traweger A, Wiggin G, Taylor L, Tate SA, Metalnikov P, Pawson T** (2008) Protein phosphatase 1 regulates the phosphorylation state of the polarity scaffold Par-3. *Proc Natl Acad Sci USA* **105**: 10402–10407
- Ueda K, Matsuyama T, Hashimoto T** (1999) Visualization of microtubules in living cells of transgenic *Arabidopsis thaliana*. *Protoplasma* **206**: 201–206
- Ulmasov T, Murfett J, Hagen G, Guilfoyle TJ** (1997) Aux/IAA proteins repress expression of reporter genes containing natural and highly active synthetic auxin response elements. *Plant Cell* **9**: 1963–1971
- Voigt B, Timmers AC, Šamaj J, Müller J, Baluška F, Menzel D** (2005) GFP-FABD2 fusion construct allows *in vivo* visualization of the dynamic actin cytoskeleton in all cells of *Arabidopsis* seedlings. *Eur J Cell Biol* **84**: 595–608
- Wang X, Zhu L, Liu B, Wang C, Jin L, Zhao Q, Yuan M** (2007) *Arabidopsis* MICROTUBULE-ASSOCIATED PROTEIN18 functions in directional cell growth by destabilizing cortical microtubules. *Plant Cell* **19**: 877–889
- Wisniewska J, Xu J, Seifertová D, Brewer PB, Ruzicka K, Blilou I, Rouquieré D, Benková E, Scheres B, Friml J** (2006) Polar PIN localization directs auxin flow in plants. *Science* **312**: 883
- Wu HM, Hazak O, Cheung AY, Yalovsky S** (2011) RAC/ROP GTPases and auxin signaling. *Plant Cell* **23**: 1208–1218
- Xu T, Dai N, Chen J, Nagawa S, Cao M, Li H, Zhou Z, Chen X, De Rycke R, Rakusová H** (2014) Cell surface ABP1-TMK auxin-sensing complex activates ROP GTPase signaling. *Science* **343**: 1025–1028
- Xu T, Wen M, Nagawa S, Fu Y, Chen JG, Wu MJ, Perrot-Rechenmann C, Friml J, Jones AM, Yang Z** (2010) Cell surface- and rho GTPase-based auxin signaling controls cellular interdigitation in *Arabidopsis*. *Cell* **143**: 99–110
- Yang Z** (2008) Cell polarity signaling in *Arabidopsis*. *Annu Rev Cell Dev Biol* **24**: 551–575
- Zhang C, Halsey LE, Szymanski DB** (2011) The development and geometry of shape change in *Arabidopsis thaliana* cotyledon pavement cells. *BMC Plant Biol* **11**: 27
- Zhou Y, Wang H, Gilmer S, Whitwill S, Fowke LC** (2003) Effects of co-expressing the plant CDK inhibitor ICK1 and D-type cyclin genes on plant growth, cell size and ploidy in *Arabidopsis thaliana*. *Planta* **216**: 604–613

Supplemental Data



Supplemental Figure S1. Tissue-specific expression of TOPP4 protein. We found that TOPP4 is expressed in leaf PCs using the *TOPP4:TOPP4-GFP* transgenic line. (A) Wild-type control, (B) *TOPP4:TOPP4-GFP* transgenic line. Scale bar = 40 μ m.



Supplemental Figure S2. The rosette leaf phenotypes of *topp4-1*.

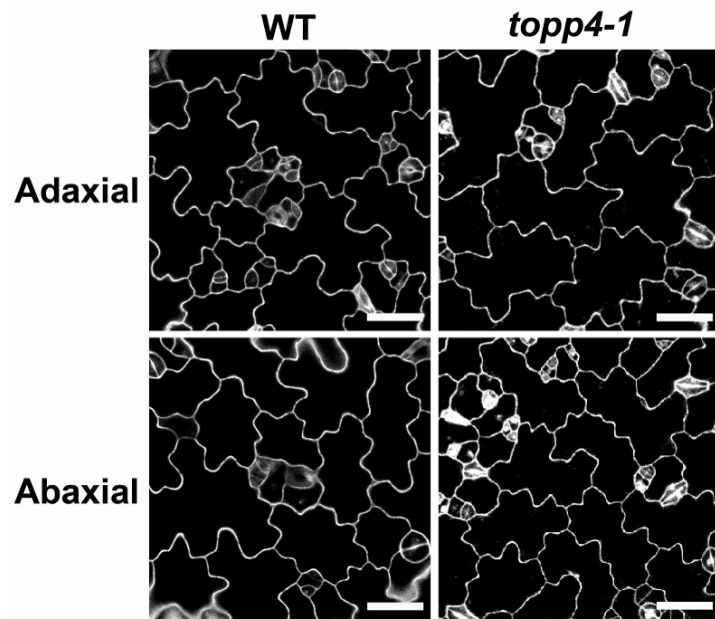
(A) The rosette leaves excised from 21-day-old wild-type plants and *topp4-1* mutants.

Scale bar = 1 cm.

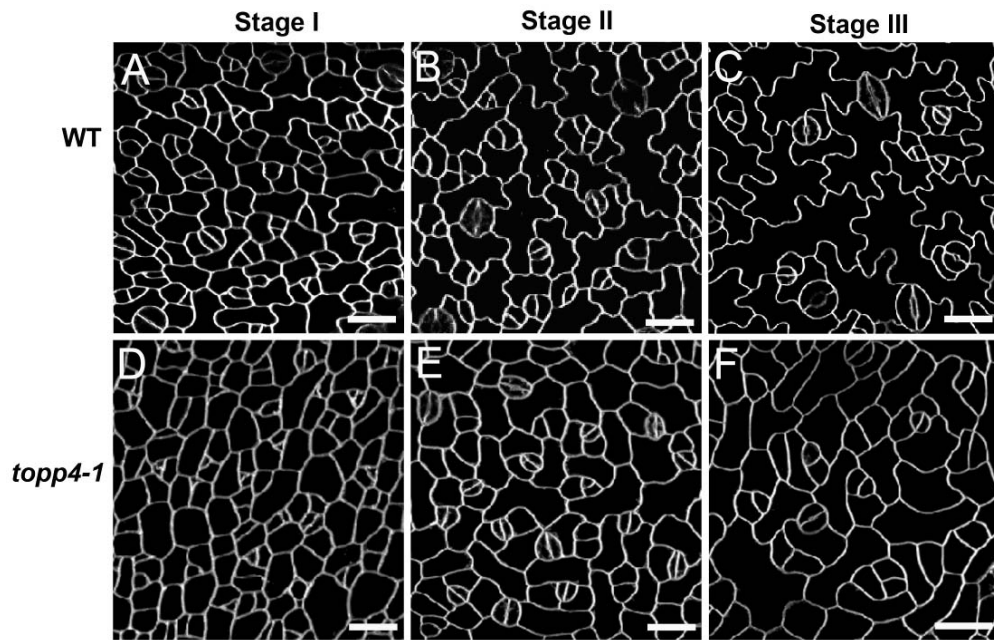
(B) and (C) Semi-thin transverse sections of the third leaves showed that more cells were formed in *topp4-1* compared to wild type. Scale bars = 10 μm .

(D) Quantitative analyses of the third leaf area.

(E) Quantitative analyses of the PC area. Asterisks in (D) and (E) represent statistic difference from wild type based on Student's *t* test with $P < 0.01$. Error bars represent SE ($n = 100$).



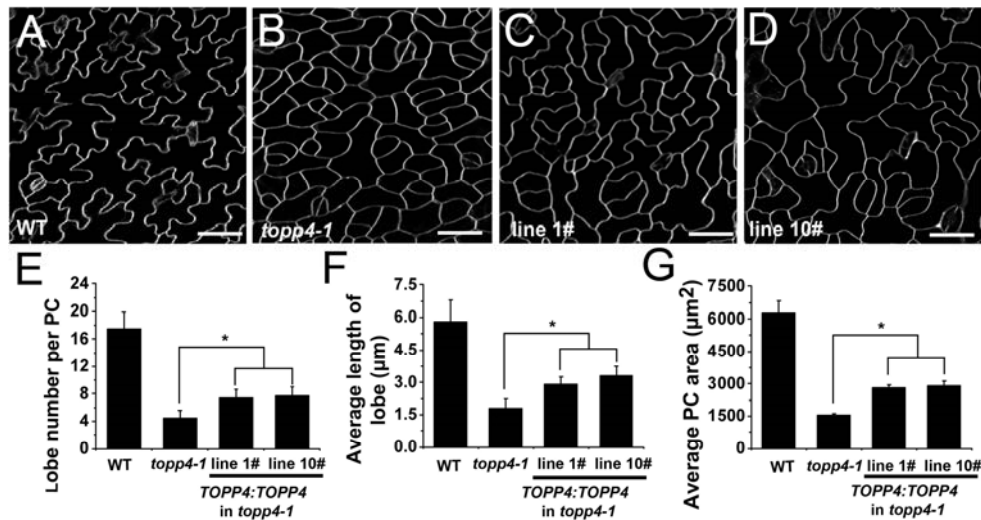
Supplemental Figure S3. The cotyledon PCs show normal shape in *topp4-1*.
Scale bars = 50 μ m.



Supplemental Figure S4. Effect of *TOPP4* mutation on PC development at different stages.

(A) –(C) Wild-type PCs on the adaxial leaf side.

(D) –(F) The *topp4-1* PCs on the adaxial leaf side. Scale bars = 50 μ m.

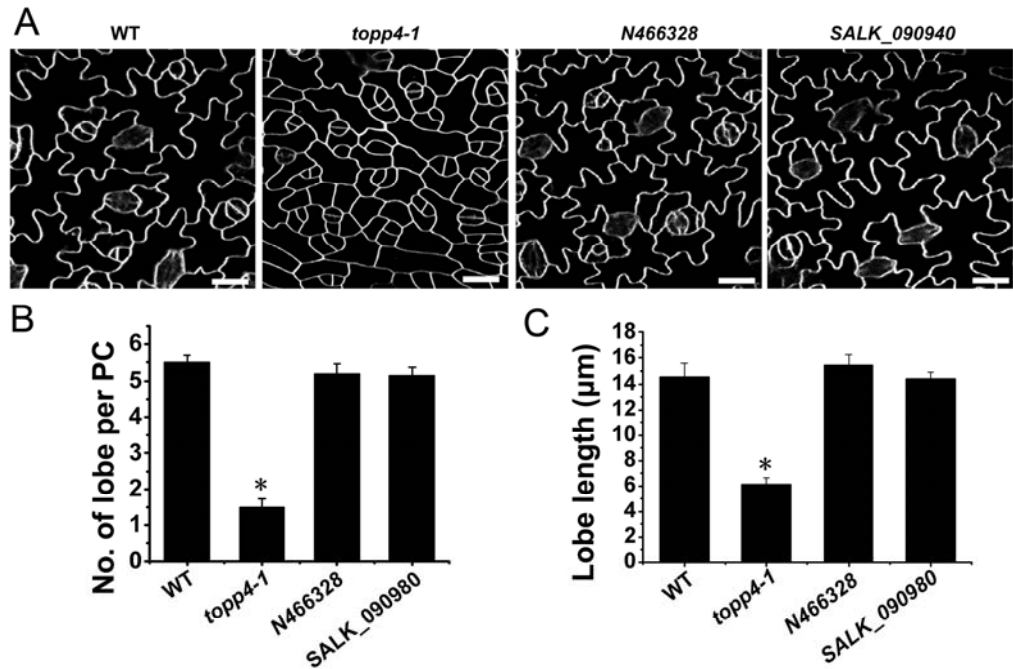


Supplemental Figure S5. Transformed *TOPP4:TOPP4* into the *topp4-1* mutant slightly rescues the mutant phenotype.

(A)–(D) The *topp4-1* mutant was transformed with *TOPP4* driven by its native promoter. The adaxial sides of the third leaves in two transgenic lines (1# and 10#) displayed shallower lobe PCs compared to wild type.

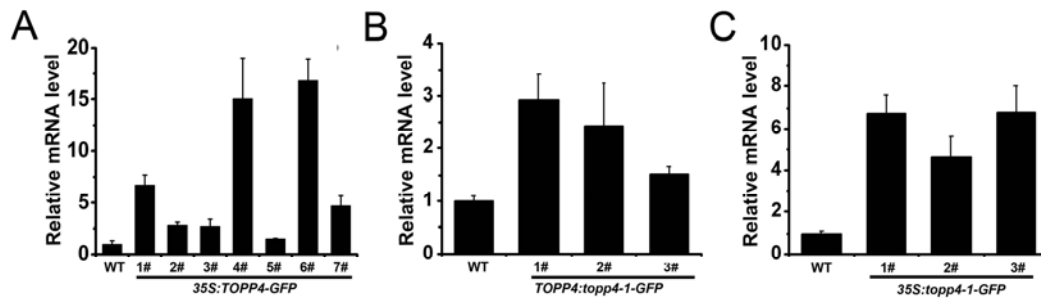
(E) and (F) Quantitative analyses of lobe number (E) and lobe length (F) in wild type, *topp4-1*, and line 1# and 10#.

(G) Quantitative analyses of the PC area in wild type, *topp4-1*, and line 1# and 10#. Asterisks in (E)–(G) represent statistic differences from the *topp4-1* mutant based on Student's *t* test with $P < 0.05$. Error bars represent SE ($n = 100$).



Supplemental Figure S6. Phenotype analysis of two T-DNA insertion alleles of *TOPP4*.
 (A) PCs on the adaxial leaf side in wild type, *topp4-1* and two T-DNA insertion lines of *TOPP4*. Scale bars = 25 μm .

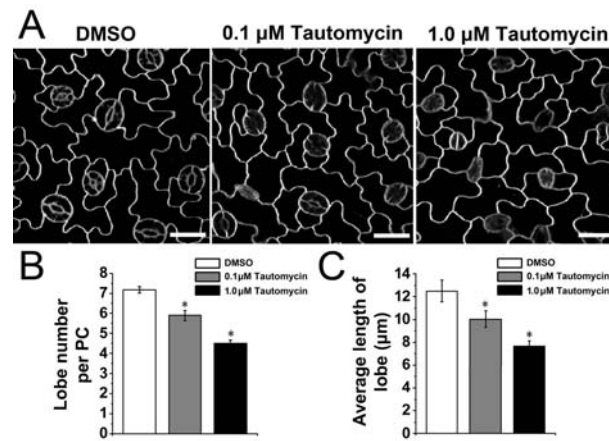
(B) and (C) Quantitative analyses of the lobe number (E) and lobe length (F) in wild type, *topp4-1* and two T-DNA insertion lines of *TOPP4*. Asterisk represents statistic difference from wild type based on Student's *t* test with $P < 0.01$. Error bars represent SE ($n = 100$).



Supplemental Figure S7. The *TOPP4/topp4-1* expression levels of the *35S:TOPP4*, *TOPP4:topp4-1-GFP*, or *35S:topp4-1-GFP* transgenic plants.

(A)The relative expression levels of the *TOPP4* in seven *35S:TOPP4* transgenic lines.
 (B)The relative expression levels of the *topp4-1/TOPP4* in three *TOPP4:topp4-1-GFP* transgenic lines.

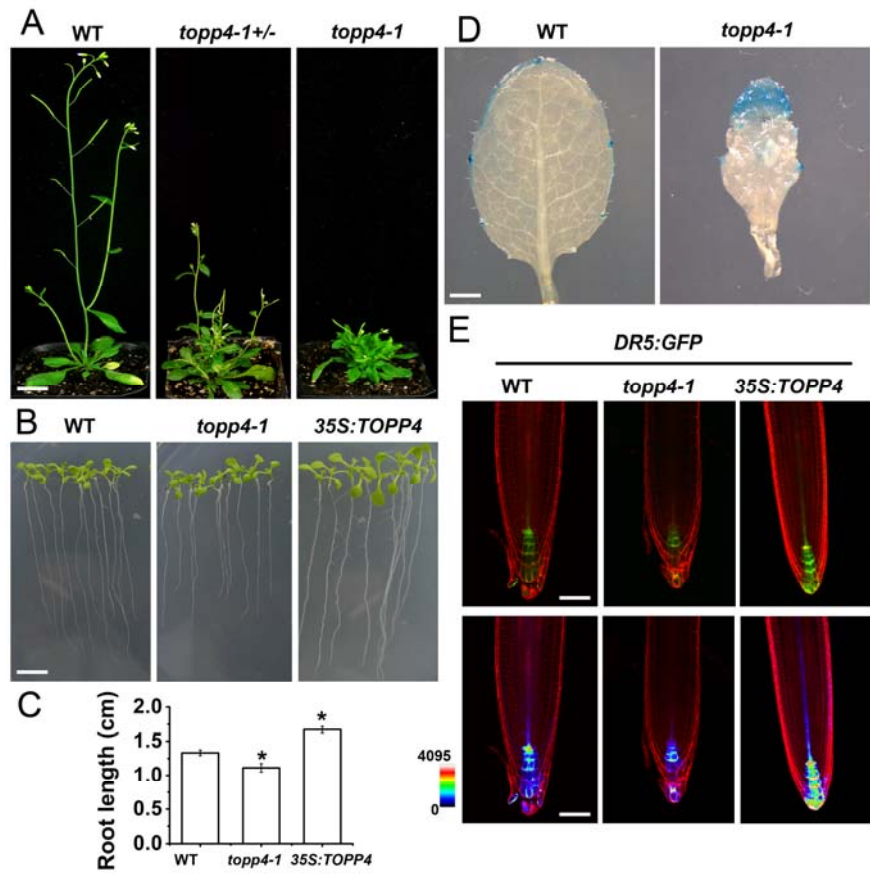
(C) The relative expression levels of the *topp4-1/TOPP4* in three *35S:topp4-1-GFP* transgenic lines. The expression level of *TOPP4* in wild type in (A)–(C) was set to 1.0.



Supplemental Figure S8. Inhibition of PP1 partially repressed interdigitated growth of PCs.

(A) The PC shape of adaxial sides of the third leaves. Scale bars = 25 μ m.

(B) and (C) Quantitative analyses of lobe number (B) and lobe length (C) of PC. Asterisks represent statistic differences from the control based on Student's *t* test with $P < 0.01$. Error bars represent SE ($n = 100$).



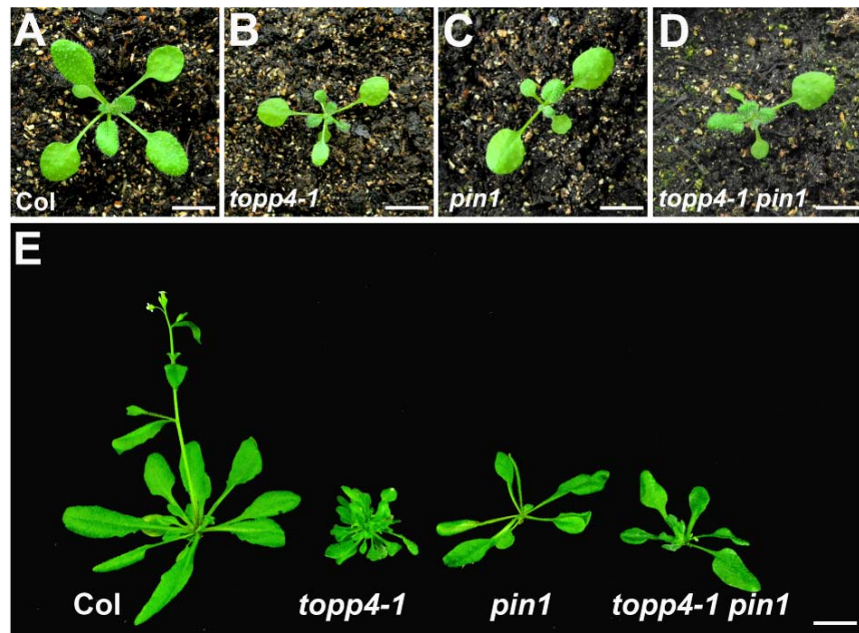
Supplemental Figure S9. The *topp4-1* mutant shows auxin-related defects.

(A) Morphology of 6-week-old wild-type, heterozygous *topp4-1+/-* and homozygous *topp4-1* seedlings. The homozygous *topp4-1* showed a lack of apical dominance and more lateral branching than wild type. Scale bar = 1.5 cm.

(B) and (C) Length of primary root on 1/2 MS medium. Scale bar = 0.5 cm. Asterisk represents statistic difference from wild type based on Student's *t* test with $P < 0.05$. Error bars represent SE ($n = 30$).

(D) The expression of the DR5-GUS signal in leaves of wild-type and *topp4-1* plants. Scale bar = 0.2 cm.

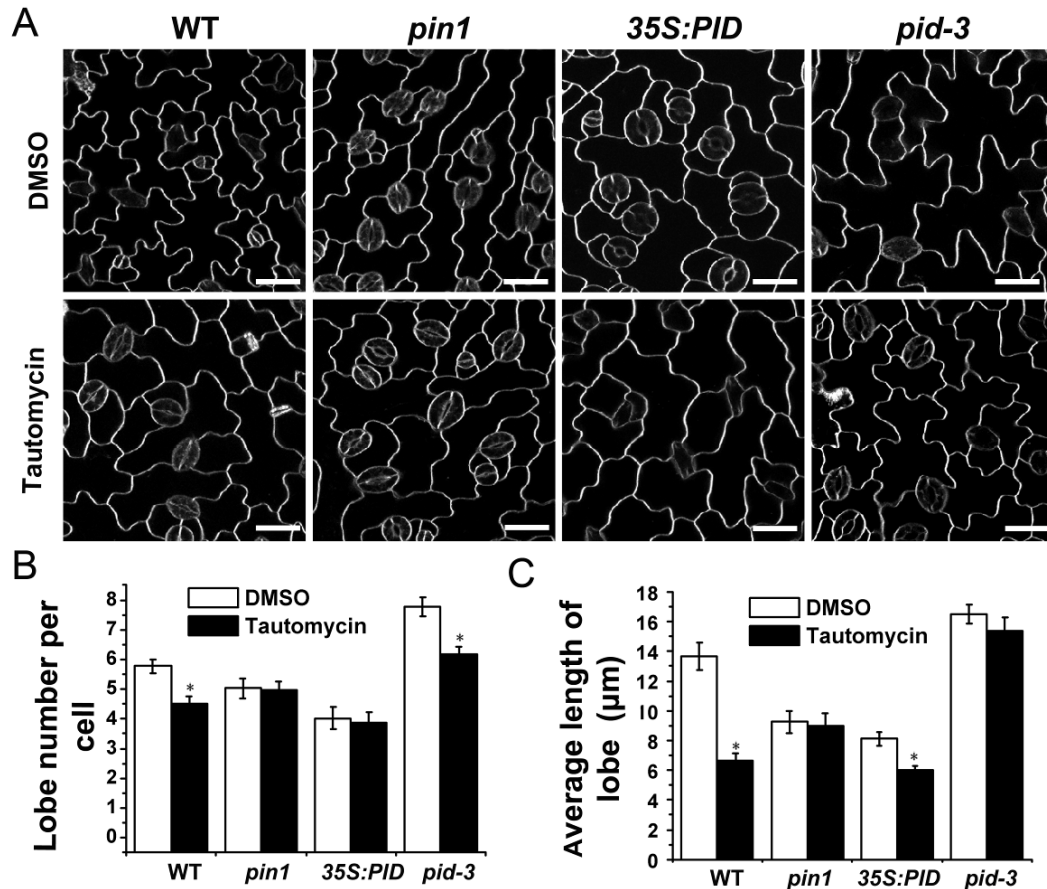
(E) The expression of the DR5-GFP signal in roots of wild-type, *topp4-1* and 35S:TOPP4 plants. Scale bars = 50 μ m.



Supplemental Figure S10. The phenotype of *topp4-1 pin1* double mutants.

(A)–(D) The leaf phenotype of 21-day-old seedlings of wild-type (A), *topp4-1* (B), *pin1* (C) and *topp4-1 pin1* (D) plants. Scale bars = 1 cm.

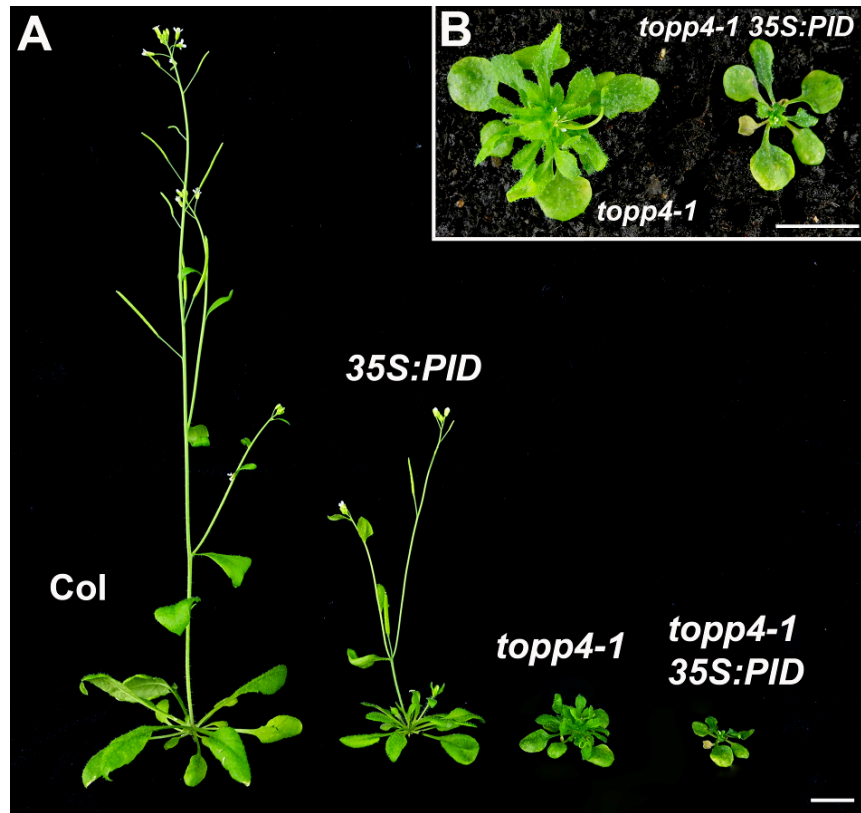
(E) The phenotype of 6-week-old seedlings of wild-type, *topp4-1*, *pin1* and *topp4-1 pin1* plants. Scale bar = 0.5 cm.



Supplemental Figure S11. Effect of tautomycin on PC shape in wild-type, *pin1*, *35S:PID* and *pid-3* plants.

(A) PCs on the adaxial side in wild-type, *pin1*, *35S:PID*, and *pid-3* plants treated with 1.0 μm tautomycin.

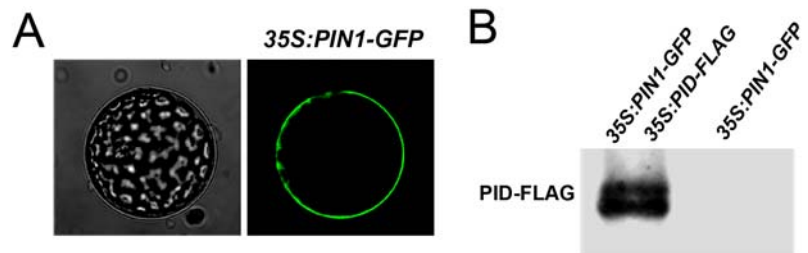
(B) Quantitative analyses of lobe number (B) and lobe length (C) of PCs in wild-type, *pin1*, *35S:PID*, and *pid-3* plants treated with 1.0 μm tautomycin. Asterisk represents statistic difference from control based on Student's *t* test with $P < 0.01$. Error bars represent SE ($n = 100$).



Supplemental Figure S12. The phenotype of *topp4-1* *35S:PID* double mutants.
(A) Seven-week-old plants.
(B) Larger image of *topp4-1* and *topp4-1* *35S:PID* plants. Scale bars = 0.5 cm.

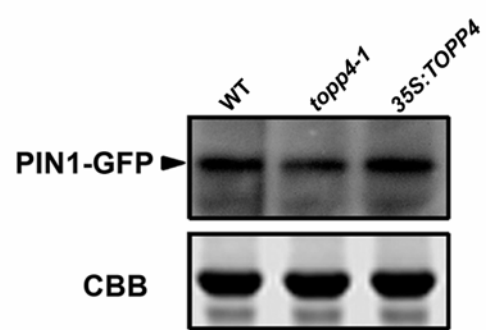


Supplemental Figure S13. The phenotype of two-month-old *topp4-1 pid-3* double mutants.
Scale bar = 2 cm.

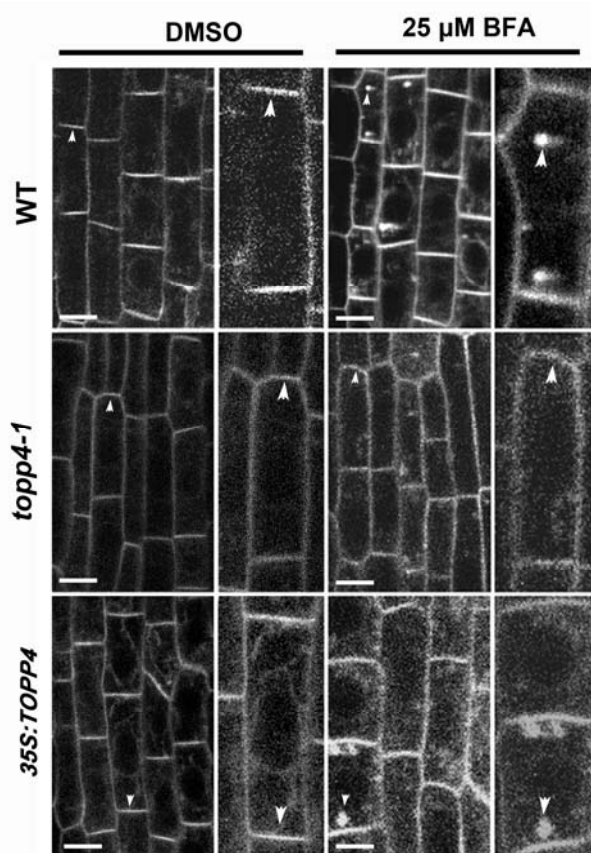


Supplemental Figure S14. Transient expression of *35S:PIN1-GFP* and *35S:PID-FLAG* in *Arabidopsis* protoplasts.

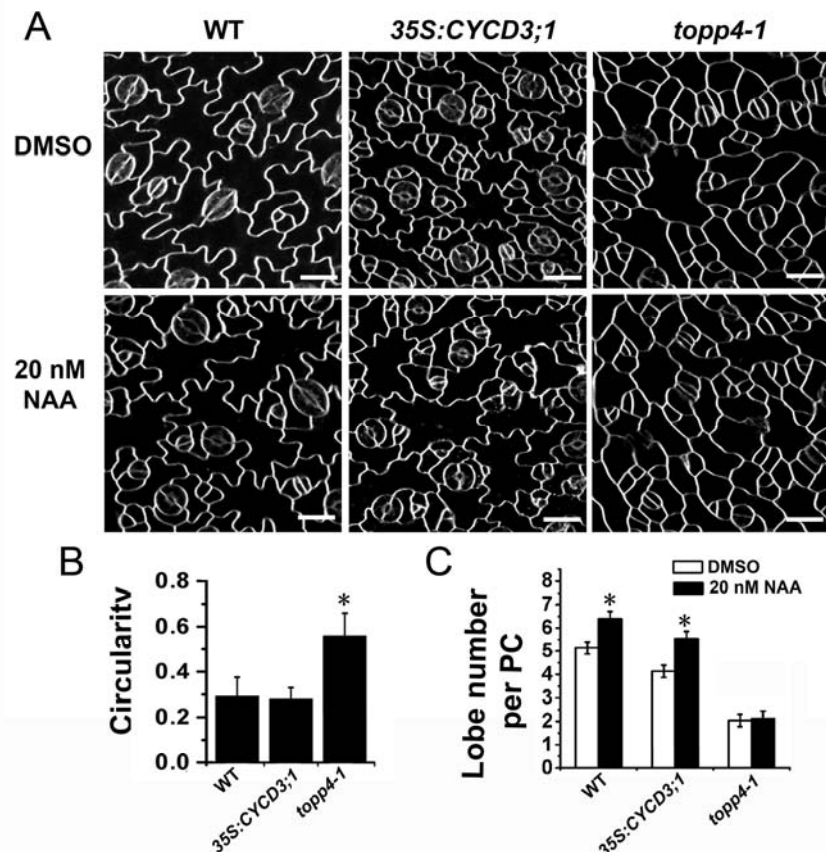
- (A) Transient expression of *35S:PIN1-GFP* in *Arabidopsis* leaf protoplasts showed that PIN1-GFP is localized predominantly to the plasma membrane.
- (B) Western blot demonstrating the PID-FLAG expression in protoplast extracts transfected with *35S:PIN1-GFP* and *35S:PID-FLAG* or without *35S:PID-FLAG* using anti-FLAG antibody.



Supplemental Figure S15. Immunoblot analyses of PIN1-GFP in wild-type, *topp4-1*, and *35S:TOPP4* plants expressing *PIN1:PIN1-GFP*.



Supplemental Figure S16. PIN1 internalization in root cells after BFA treatment.
Arrowheads represent the most pronounced localization of PIN1 at the apical/basal cell side or in BFA bodies. Scale bars = 10 μ m.

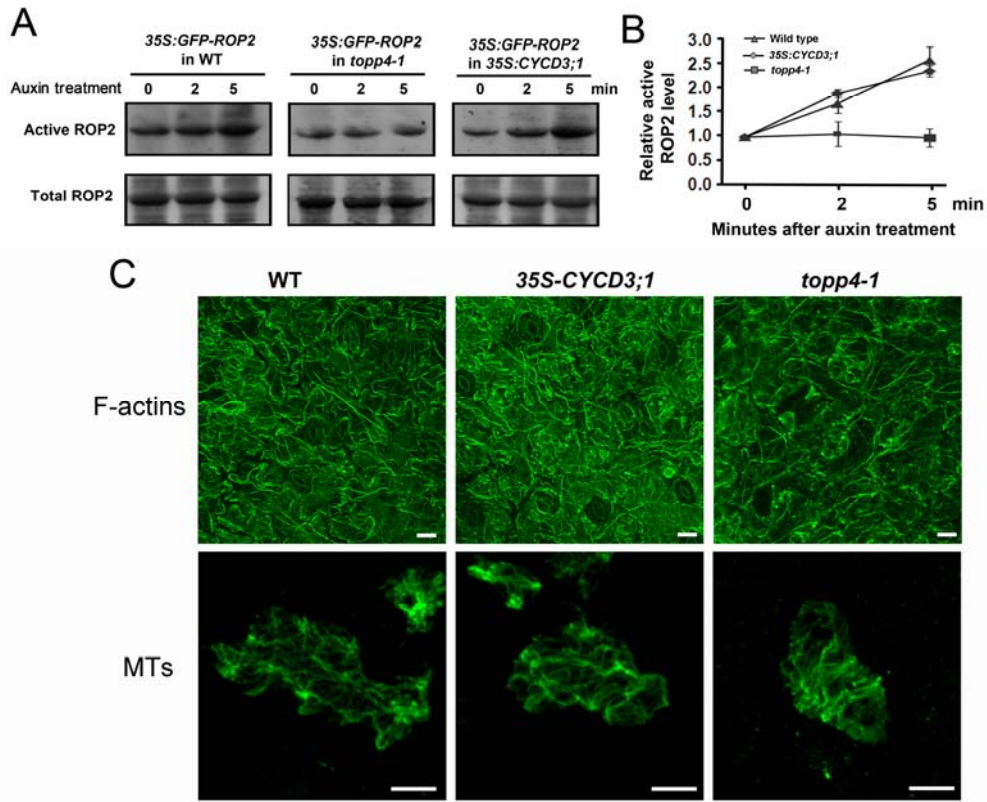


Supplemental Figure S17. The effect of exogenous auxin on the PC lobe formation in *35S:CYCD3;1*.

(A) PCs on the adaxial leaf side in wild-type, *35S:CYCD3;1* and *topp4-1* plants treated with DMSO or 20 nM NAA. Scale bars = 20 μ m.

(B) The circularity values of PCs in wild-type, *35S:CYCD3;1* and *topp4-1* plants.

(C) Analyses of lobe number per PC in wild-type, *35S:CYCD3;1* and *topp4-1* plants treated with DMSO or 20 nM NAA. Asterisks in (B) and (C) represent statistic differences from wild type based on Student's *t* test with $P < 0.01$. Error bars represent SE ($n = 100$).



Supplemental Figure S18. The effect of auxin on ROP2 activity and the organization of cortical MTs and F-actins in 35S:CYCD3;1.

(A) Measurements of GTP-bound ROP2 activity in wild-type, 35S:CYCD3;1 and *topp4-1* protoplasts transiently expressing 35S:GFP-ROP2.

(B) Quantitative analyses of the relative active ROP2 activity. Error bars represent SE ($n = 3$).

(C) The organization of cortical MTs and F-Actins in the PCs of wild-type, 35S:CYCD3;1 and *topp4-1*. Scale bar= 20 μ m.

Supplemental Table S1. Primers used for plasmid construction and qRT-PCR.

Primer Name	Sequence
<i>pid-3</i> -F	TTAGCTAATGAGTATTATTTTG
<i>pid-3</i> -R	AAGATTCAACGGCTGCG
<i>pin1</i> -F	CAAAAACACCCCCAAAATTTC
<i>pin1</i> -R	AATCATCACAGCCACTGATCC
<i>topp4-1</i> -F	ATGGCGACGACGACGAC
<i>topp4-1</i> -R	TCCTCCTCCAATCTTGTG
<i>pA7:PIN1</i> -F	GCGTCGACATGATTACGGCGGCGAC
<i>pA7:PIN1</i> -R	CGGGATCCTAGACCCAAGAGAAATGTAG
<i>pA7:RIC1</i> -F	GTCGACATGGCGACGGACAATGAAG
<i>pA7:RIC1</i> -R	GGATCCGATAATATCGTTACAGG
<i>pA7:RIC4</i> -F	GTCGACATGAGAGATAGAATGGAG
<i>pA7:RIC4</i> -R	GGATCCTAAAGTTGGATGAAGATG
<i>ROP2</i> -RT-F	CTGGTGTCCCATTATCCTTG
<i>ROP2</i> -RT-R	CCTCTCCCTGGTTTAGTA
<i>ROP4</i> -RT-F	CACTTCCCTACGGACTATG
<i>ROP4</i> -RT-R	CACGGTAACTCAACGGTCTT
<i>ROP6</i> -RT-F	CCACGGATTATGTGCCAACTG
<i>ROP6</i> -RT-R	ATCTGCACCGCGATAGCTCA